CALBINDIN AND CHANNELRHODOPSIN-2 EXPRESSION IN THE DOPAMINERGIC SNC AND VTA OF DAT-CRE::CHR2-EYFP MICE

by

Olivia Waller

A thesis submitted in partial fulfillment of the requirements for the degree of

BACHELOR OF SCIENCE, HONOURS

Department of Biology

University of Victoria

April 2023

Supervisory Committee:

Dr. Raad Nashmi, Department of Biology
Supervisor

Dr. Barbara Hawkins, Department of Biology
Honours Advisor

Dr. Nicole Templeman, Department of Biology
External Examiner

Abstract

The DAT-Cre::ChR2-EYFP mouse model has recently emerged as a useful tool to investigate the function of the dopaminergic (DA) system, which is known to be involved in motor behaviour, motivation and reward, memory, and cognition. This is accomplished through selective expression of channelrhodopsin-2 (ChR2), a blue light-activated cation channel, in DA neurons. DA neurons that express calbindin (Calb), a calcium-binding protein, make up a discrete subpopulation with unique functional characteristics. Functional and physiological heterogeneity between the substantia nigra pars compacta (SNc) and ventral tegmental area (VTA) has been well documented, and past research conducted by the Nashmi lab has observed physiological heterogeneity between DA neurons along the mediolateral axis of the SNc itself. Therefore, there may be potential for Calb to act as a marker for distinct physiological cell phenotypes. Here, we evaluate the DAT-Cre::ChR2-EYFP model's efficiency in expressing ChR2 within DA neurons and characterize the colocalization of Calb in DA neurons within the VTA and along the mediolateral axis of the SNc. We used confocal fluorescence microscopy of DAT-Cre::ChR2-EYFP brains and quantified tyrosine hydroxylase (TH), ChR2, and Calb expression within regions of interest. No significant difference in Calb colocalization in DA neurons was found between the medial and lateral SNc, although a large difference was observed between the SNc and VTA. We also report a that the DAT-Cre::ChR2-EYFP mouse model is extremely efficient in expressing ChR2 in DA neurons of the midbrain.

Table of Contents

List of Figures

List of Tables

Acknowledgements

Firstly, I would like to thank my supervisor Dr. Raad Nashmi for accepting me as a volunteer into the Nashmi Lab, and for your subsequent support and mentorship throughout the course of my Honours project. Being a part of your lab has tremendously enriched my scientific education, and I'm sure the many skills I gained here will prove invaluable as I move into my future endeavors. I will always look back at my time in your lab very fondly.

Thank you to Dr. Nicole Templeman and Dr. Barbara Hawkins for being on my committee. I have learned so much from this project, and I really appreciate you taking the time to review the final product of my work.

A very big thank you to Penelope Young for all your guidance throughout my time in the lab. Your constant reassurance and insight were indispensable in helping me navigate the highs and lows of my research. I couldn't have done this project without you.

I would also like to thank all the other members of the Nashmi Lab, for their continuous contribution and dedication to the lab.

A final thanks to my family, as well as my friends Danielle and Vicka, for being there for me throughout my undergraduate degree and life. Without your support and love, I would not have been able to achieve all that I have today.

1.0 Introduction

1.1 Dopamine and the DA system

3,4-dihydroxyphenethylamine, the molecule that would later become known as dopamine, was first synthesized in 1910 by researchers George Barger and James Hill and soon after characterized by Henry Dale as a monoamine similar to norepinephrine (Hornykiewicz, 2002). It was widely thought that dopamine functioned solely as a precursor to norepinephrine until landmark research performed by Carlsson *et al.,* (1957), which established that dopamine also functioned as an independent neurotransmitter. The role of dopamine in the central nervous system has now been extensively researched. Dopamine is known to play integral roles in reward-motivated learning, locomotion, cognitive function, reinforcement, memory, attention, and emotion (Adcock *et al.,* 2006; Badgaiyan *et al.,* 2010; Dang *et al.,* 2012; Howe and Dombeck, 2016; Kravitz *et al.,* 2012; Nagano-Saito *et al.,* 2008; Schultz *et al.,* 1993, Schultz *et al.,* 1997). It is also known to be involved in mental health disorders such as addiction, attention deficit hyperactivity disorder, and schizophrenia, in addition to neurodegenerative disorders Parkinson's disease and Huntington's disease (Bäckman et al., 1997; Ehringer and Hornykiewicz, 1998; Rung et al., 2005; Volkow et al., 1993; Volkow et al., 2009). In the periphery, dopamine is secreted from neurons, the adrenal medulla, and neuroendocrine cells and plays a role in sympathetic activity, glucose homeostasis, and immune functioning (Rubí and Maechler, 2010).

The first step of the synthesis of dopamine occurs in the liver, where the amino acid tyrosine is catabolized to L-tyrosine by the enzyme phenylalanine hydroxylase. L-tyrosine then travels to the brain through the bloodstream for use in the central nervous system (Best *et al.,* 2009; Katolikova and Gainetdinov, 2022). Dopamine is mainly produced in the VTA and SNc, the major DA nuclei of the brain (Poulin *et al.,* 2018). Tyrosine hydroxylase catalyzes the conversion of L-tyrosine to L-DOPA, the rate-limiting step of dopamine synthesis. Finally, aromatic L-amino acid decarboxylase converts L-DOPA into dopamine, which is released in vesicles from the presynaptic terminal of DA neurons upon firing (Best *et al.,* 2009; Katolikova and Gainetdinov, 2022).

Subpopulations of DA neurons project from the SNC and VTA to make up three major DA pathways of the central nervous system, the nigrostriatal, mesolimbic, and mesocortical pathways. DA neurons from the SNc project to the dorsal striatum, forming the nigrostriatal pathway which is involved in locomotion and motor control (Haber, 2014; Wüllner *et al.,* 1994).

Projections from the VTA that innervate the nucleus accumbens in the ventral striatum constitute the mesolimbic pathway, which is involved in reward and motivation (Everitt *et al.,* 1991; François *et al.,* 1999). The mesocortical pathway plays a role in cognition and is comprised of VTA neurons that project to the cerebral cortex (Papenberg *et al.,* 2019; Willing and Wagner, 2016). A fourth DA pathway, the tuberoinfundibular pathway, does not originate in the midbrain; instead, it projects from the hypothalamus to the median eminence to inhibit prolactin secretion from the anterior pituitary gland (Katolikova and Gainetdinov, 2022; Stagkourakis *et al.,* 2019).

To modulate these processes, dopamine binds to DA receptors in the central nervous system and periphery. Dopamine receptors are G-protein coupled receptors, and therefore exert their effects on a cell through G-protein activation (Zhou *et al.,* 1990). There are 5 subtypes of dopamine receptors, and these subtypes are grouped into two classes: D1-like (D1 and D5) and D2-like (D2, D3, and D4) (Garau *et al.,* 1978). D1-like receptors activate an adenylyl cyclase signalling cascade, increasing levels of cAMP synthesis and activating PKA, while D2-like receptors inhibit adenylyl cyclase and therefore decrease levels of cAMP and PKA (McDonald *et al.,* 1984; Zhou *et al.,* 1990). Dopamine receptor activity is eventually stopped through phosphorylation of the receptor by GPCR kinases and subsequent inhibition and internalization facilitated by the binding of arrestin proteins (Gurevich and Benovic, 1993; Palczewski *et al.,* 1991).

1.2 Parkinson's disease

Parkinson's disease is the most common neurodegenerative disease after Alzheimer's disease, and studies have shown that its prevalence continues to grow at a steady rate (Ou *et al.,* 2021; Willis *et al.,* 2022). This disease is characterized by death of DA neurons in the SNc, resulting in decreased dopamine levels in the brain that cause motor deficits such as tremors and loss of voluntary muscle movement (bradykinesia) (Bernheimer *et al.,* 1973). These motor deficits observed in Parkinson's disease are due to cell death of nigrostriatal DA neurons (Wüllner *et al.,* 1994). Although degeneration in the VTA has also been observed, cell death in the SNc is much more severe (Alberico *et al.* 2015). Parkinson's disease involves the aggregation of mutated α-synuclein, a presynaptic neuronal protein that is thought to normally function in neurotransmitter release through modulating assembly of the SNARE complex, into masses called Lewy bodies

(Stefanis, 2012). There has been evidence to suggest that α-synuclein also plays a role in calcium homeostasis, such that when α-synuclein is mutated and forms Lewy bodies this homeostasis is disrupted and increases the vulnerability of DA neurons to cell death (Calì *et al.,* 2012).

The bradykinesia experienced by those living with Parkinson's disease is due to dysregulation of two major pathways originating from the basal ganglia. These direct and indirect pathways are involved in motor control and modulated by dopamine levels produced by the SNc. Medium spiny neurons (MSNs) in the direct pathway express D1 receptors and are therefore excited by DA exposure, while MSNs in the indirect pathway that express D2 receptors are inhibited by DA (Gerfen *et al.,* 1990). The direct pathway acts to facilitate voluntary movements through disinhibition of the thalamus. On the other hand, the indirect pathway works to counteract the disinhibitory action of the direct pathway, enabling one to inhibit unwanted movement and have fine-tuned control over motor behaviours (Kravitz *et al.,* 2010; Onla-or and Winstein, 2001). The loss of DA seen in Parkinson's disease results in less activation of the direct pathway and therefore less initiation of movement. At the same time, DA loss leads to less inhibition of the indirect pathway and thus even more inhibition of movement (Onla-or and Winstein, 2001).

1.3 Channelrhodopsin-2

Channelrhodopsin-2 (ChR2) is a nonselective cation channel that is activated by stimulation with blue light (450-490 nm) (Nagel *et al.,* 2003). It was derived from the green algae *Chlamydomonas reinhardtii,* which had been observed to change its swimming direction in reaction to light. This was found to be due to an inward current in the flagella regions of cells, caused by rhodopsin-mediated channel opening; ChR2 was one such rhodopsin (Harz and Hegemann, 1991). ChR2 is activated by blue light through photon absorption by an all-*trans* retinal chromophore. Upon this activation, ChR2 undergoes large conformational changes in its protein backbone brought about by a *trans-cis* isomerization of the retinal, leading to the opening of the channel. Cations are then allowed to flow down their electrochemical gradients. Eventually the receptor becomes desensitized, the retinal reverts to an all-*trans* retinal configuration, and the protein backbone relaxes which leads to channel closing and conclusion of signal transduction. ChR2 has a relatively long open period, with the time the channel remains open in the range of seconds. This contributes to the high efficiency and large conductance of ChR2s but could also result in poorer temporal

resolution as ChR2 may be less able to encode rapid changes in signals than other channels (Hight *et al.,* 2015; Nagel *et al.,* 2003; Radu *et al.,* 2009). In neurons, the resting membrane potential is -70 mV and the ChR2-mediated influx of cations into the cell results in depolarization. If the depolarization threshold is met, an action potential will be generated, and the cell will fire (Boyden *et al.,* 2005).

Although ChR2 is of microbial origin, when artificially expressed in animals it can be used in a technique called optogenetics, wherein the effect of light stimulation can be used to examine the activity of particular neurons or brain regions (Boyden *et al.,* 2005). Conditional expression of ChR2 in specific tissues or cell types can be achieved using cre recombinase-dependent transgenics or through introduction of adeno-associated viruses. Through these methods, researchers can decipher the physiological roles of certain brain areas and neural circuits (Gompf *et al.,* 2015; Madisen *et al.,* 2012). Optogenetics involves the implantation of a light source into a region of interest that expresses an opsin such as ChR2. When stimulated by light, opsin-expressing neurons will become activated and fire an action potential to their downstream targets (Boyden *et al.,* 2005) (Fig 1). DAT-Cre::ChR2 mice can be used to facilitate the expression of ChR2 selectively in DA neurons, allowing one to examine the effects of DA stimulation on various processes (Fig 2) (Bäckman *et al.,* 2006; Madisen *et al.,* 2012). However, this model has not, to the best of our knowledge, been evaluated in its efficacy in expressing ChR2 in DA neurons. As sufficient ChR2 expression is needed to successfully impact neuronal function and maximize the potential use of this model for optogenetic research, quantifying the level of colocalization of ChR2 in DA neurons in the major DA nuclei (SNc and VTA) of DAT-Cre::ChR2-EYFP mice would help to shed more light on this model's efficacy and reliability (Britt *et al.,* 2013).

In addition to helping decipher the functions of specific neuronal types and pathways, optogenetic techniques that harness ChR2 have also recently been viewed as an avenue for potential treatment of neurological disorders. Introduction of light-activated ChR2 into retinal neurons has been shown to restore vision in mice with photoreceptor degeneration, such as that seen in retinitis pigmentosa (Bi *et al.,* 2006). In the context of spinal cord injuries, blue light stimulation of ChR2 has enabled paralyzed motor nerves in the diaphragm to act in an unparalyzed manner (Alilain *et al.,* 2008). A common treatment for Parkinson's disease is L-DOPA; however, while this treatment slows the degradation of SNc DA neurons seen in the disease, it is also

accompanied by the appearance of motor fluctuations and dyskinesia (Rascol *et al.,* 2000). One recent study stimulating implanted ChR2-expressing stem cells reported alleviation of these locomotor impairments (Zenchak *et al.,* 2018). Another found that ChR2-mediated activation of the medium-spiny neurons of the direct pathway of the basal ganglia in a mouse model of Parkinson's disease lessened locomotor deficits and bradykinesia (Kravitz *et al.,* 2010). Therefore, evaluation of transgenic models that harness ChR2 as means to activate certain cell populations contributes valuable information for the development of various therapeutic strategies for neurodegenerative diseases. Knowing the efficacy of the DAT-Cre::ChR2-EYFP model in particular would be important for future optogenetic therapies that selectively target DA neurons.

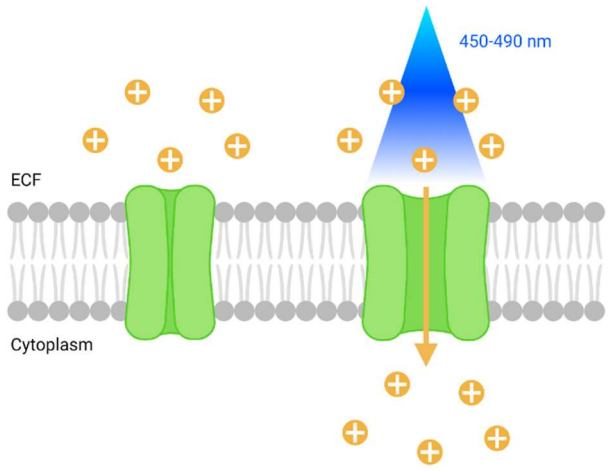

Figure 1. ChR2 activation. ChR2 resides on the membrane of a cell. When inactive, it is closed and does not facilitate any ion flux. Upon stimulation with blue light (nm = 450-490), ChR2 undergoes a conformational change and opens, allowing for cation flux down the electrochemical gradient. When expressed in neurons, this facilitates an influx of cations, leading to depolarization and action potential firing.

1.4 Calbindin

Calbindin (Calb) is a calcium-binding protein that plays various roles in animal physiology, mainly in the absorptive epithelium and central nervous system where it acts as a buffer, sensor, and transporter for calcium (Schmidt, 2012). Within the intestine, it is well-established that Calb plays a role in vitamin D-mediated calcium absorption (Lambers *et al.,* 2006). Calb's presence in the nervous system is vital in maintaining calcium homeostasis and is also thought to play a role in

preventing cell death (Chard *et al.,* 1993; Christakos *et al.,* 1990). The calbindin protein contains four binding sites at which calcium can bind with high affinity (Veenstra *et al.,* 1997). Calb resides in the cytoplasm of a cell and maintains calcium homeostasis by acting as a buffer to bind excess intracellular calcium (Chard *et al.,* 1993). In both apo and Ca^{2+}-bound forms, Calb interacts with various proteins within the cell; however, upon Ca^{2+} binding Calb undergoes a large conformational change that modifies the proteins with which it can interact and the affinity with which it binds its targets (Kojetin *et al.,* 2006). Therefore, Calb can have varying intracellular functions depending on physiological conditions such as intracellular Ca2+ concentration, and in this way also acts as a calcium sensor. Calb has also been observed to act as a transporter by mediating buffered calcium diffusion across the spine neck that connects dendrite shafts with the head region of dendritic spines to mediate spinodendritic cross talk (Schmidt *et al.,* 2005).

Calb has largely been emphasized as a factor contributing to resistance to cell death seen in various diseases. Studies have observed that the presence of Calb in a cell is helpful in binding excess intracellular calcium that would otherwise trigger various apoptotic cell death cascades (Rintoul *et al.,* 2001). It is also thought that Calb prevents death by directly inhibiting a common downstream effector molecule in many apoptotic pathways, caspase-3 (Christakos and Liu, 2004). In particular, Calb has been singled out as a marker for neurons with higher resistance to cell death experienced in the nervous system during Parkinson's disease. As previously described, in Parkinson's disease the SNc degenerates to a much larger degree than the VTA; this has been correlated with higher expression of Calb in the VTA as compared to the SNc (Reyes *et al.,* 2012). Within the SNc, Yamada *et al.* (1990) found surviving neurons corresponded with positive Calb expression in humans when comparing Parkinsonian brains to control brains. In another study, researchers observed increased α -synuclein accumulation as well an increase in apoptosis in neurons of Calb knock-out mice (Jung *et al.,* 2020). While this research indicates that the absence of Calb leaves a neuron more vulnerable to cell death, further research has demonstrated that induced expression of Calb in cells where it is normally absent provides a neuroprotective effect. Vitamin-D mediated induction of Calb expression has been shown to decrease α-synuclein formation in human neuroblastoma cells experiencing raised levels of intracellular Ca^{2+} (Rcom-H'cheo-Gauthier *et al.,* 2017). In monkeys, induced Calb expression has also shown to protect against Parkinsonian-like neuronal death in the substantia nigra caused by the administration of MPTP, a toxin selective to nigrostriatal DA neurons (Inoue *et al.,* 2018). Thus, Calb may not only

protect neurons that already express it from apoptotic cell death, but ectopic expression of Calb may allow those neurons previously vulnerable to such death to be spared.

1.5 Heterogeneity in midbrain DA neurons

The DAT-Cre mouse strain is commonly used to examine the activation or inhibition of many DA areas or subpopulations; however, interpreting the results of this activity becomes more complicated when considering the heterogeneity within DA populations. That said, a more complete understanding of this heterogeneity could enable the development of subpopulation-specific mouse models which could be used to examine selective activation/inhibition of these subpopulations (Anderegg *et al.,* 2016).

Calb+ DA neurons have been characterized as a functionally distinct group of DA neurons. They have been shown to differ from Calb- DA neurons in their resistance to cell death as previously mentioned, but also in their firing properties, susceptibility to excitatory/inhibitory DA input, calcium-channel composition, and levels of dopamine release and uptake (Brimblecombe *et al.,* 2019; Evans *et al.,* 2017). Expression of Calb in DA neurons also influences where they project in the striatum (Gerfen *et al.,* 1987). The expression of Calb in DA neurons is known to be significantly higher in the VTA compared to the SNc as a whole. Many studies characterize the dorsal SNc as Calb+, while the ventral SNc is Calb- (Anderegg *et al.* 2016; Fu *et al.,* 2012). Interestingly, this is correlated with an increased resistance of the dorsal SNc to Parkinsonian cell death as compared to the ventral SNc (Gibb and Lees, 1991). The consensus on DA neuron Calb expression along mediolateral axis of the SNc, however, has not been reached and existing research offers variable results. Fu *et al.* (2012) found that the lateral SNc of mice had much higher Calb/tyrosine hydroxylase (TH) co-expression than the medial SNc. However, the opposite has been observed in humans (Yamada *et al.,* 1990) and rats (Nemoto *et al.,* 1999). It is noteworthy that DA neurons in the medial SNc demonstrate heightened resistance to cell death compared to the lateral (Damier *et al.,* 1999; Fearnley and Lees, 1991). Since Calb is theorized to be implicated in cell death resistance one might expect the medial SNc to contain higher proportions of Calb+ DA neurons.

Researchers have also observed that the medial and lateral SNc have distinct physiological properties. DA neurons in the medial SNc have been found to receive mainly inhibitory input, while the lateral DA SNc receives excitatory input (Estakhr *et al.,* 2017). There have also been observed differences in locomotor control; activation of the medial SNc inhibits locomotion, while activation of the lateral SNc increases it (Estakhr *et al.,* 2017). Furthermore, lesions in the medial or lateral SNc produce circling behaviours in opposite directions (Franklin and Wolfe, 1987). Calb may be implicated in physiological heterogeneity in the midbrain through its effect on energy-activated potassium channels (K-ATP channels). Activation of K-ATP channels promotes burst firing in medial DA neurons in the SNc (Schiemann *et al.,* 2012). In mice, this firing pattern has been associated with novelty-induced exploration behaviour (Schiemann *et al.,* 2012). It has been theorized that the presence of Calb promotes this burst firing through its calcium buffering capabilities (Knowlton *et al.,* 2018). Therefore, characterizing the expression of Calb along the mediolateral axis of the mouse midbrain may help establish Calb as a marker for physiologically- and functionally-distinct DA populations.

1.6 Study objectives and hypotheses

This study has two major objectives. First, we aim to evaluate the efficiency of the DAT-Cre::ChR2-EYFP transgenic mouse model in expressing ChR2 in DA neurons in the SNc and VTA. Second, we aim to characterize the expression of Calb in DA neurons in the VTA and along the mediolateral axis of the SNc. We hypothesize that every DA neuron analyzed will express ChR2, as theoretically the Cre-lox system used will conditionally drive ChR2 expression solely in DA neurons. We also hypothesize that the medial SNc will show greater levels of Calb colocalization in DA neurons as compared to the lateral SNc.

2.0 Materials and Methods

2.1 Animal care and breeding

Experiments conducted in this study were in accordance with the University of Victoria Animal Care Committee's animal care and use protocols, following guidelines set by the Canadian Council on Animal Care (CCAC). Mice were raised at the Animal Care Unit of the University of Victoria.

They were socially housed under a 12-hour light/dark cycle and were provided with food and water *ad libitum.*

The DAT-Cre::ChR2-EYFP mouse strain used in this study was bred by crossing two strains of knock-in mice, DAT-Cre (Bäckman *et al.,* 2006) (JAX stock# 006660) and ChR2-EYFP (Madisen *et al.,* 2012) (JAX stock# 024109), until heterozygosity for DAT-Cre and homozygosity for Ai32(RCL-ChR2(H134R/EYFP) was achieved. DAT-Cre knock-in mice express cre recombinase through activation of the dopamine transporter (*DAT*) promoter. ChR2-EYFP knock-in mice possess a *loxP*-flanked STOP cassette prior to a ChR2-EYFP construct, inserted into the *ROSA26* locus. In the DAT-Cre::ChR2-EYFP mice used here, the *loxP*-flanked STOP cassette was deleted only in cre-expressing DA neurons, allowing for ChR2-EYFP expression selective to DA (*DAT*-expressing) neurons (Fig 2). Two male and two female mice were used during the study, and the ages of mice used ranged from 8 to 24 weeks.

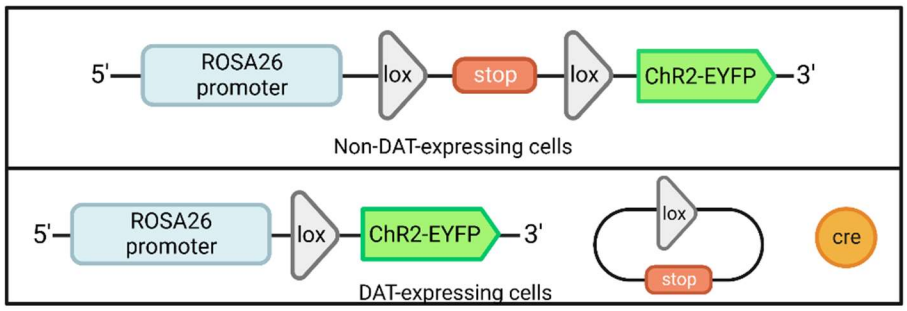

Figure 2. The Cre-lox system in DAT-Cre::ChR2-EYFP mice. In non-DA neurons, cre recombinase is not expressed and the stop codon preceding the ChR2-EYFP transgene remain in the gene, stopping transcription before this transgene is reached. In DA cells, cre recombinase will cut at *loxP* sites flanking the stop codon, excising it and allowing transcriptional machinery to reach the transgene. This results in ChR2-EYFP expression selectively in DA cells.

2.2 Immunohistochemistry

Figure 3 shows the methodology used to prepare brains for data collection. Solutions for perfusion, sectioning and immunohistochemical staining were prepared within a week of use. Mice were anesthetized with isofluorane (Fresenius Kabi, product# CP0406V2) and once sedated underwent a transcardial perfusion. The perfusion was carried out with 20 mL phosphate buffer saline (PBS), followed by 25 mL 4% paraformaldehyde (PFA) (in PBS, pH 7.4) delivered through a peristaltic pump at a rate of 4 mL/min (Masterflex Easy Load, Cole-Parmer, cat#EW-07518-00). The brain

was dissected out after the perfusion and transferred into a 4% PFA solution (in PBS, pH 7.4) overnight before being transferred into PBS. The brain was stored at 4°C from perfusion until sectioning. Sectioning was performed within a week of perfusion of the brain. Once removed from the PBS solution, the cerebellum and olfactory bulbs of the brain were removed using a razor blade and the brain was place rostral-side-up in a weigh boat. It was then submerged in 1.5% agar (Thermo Fisher Scientific, cat#BP1423500) (in PBS, pH 7.4) and allowed 10 minutes to solidify prior to sectioning. 100 µm coronal sections ranging from -3.28 to -3.62 bregma (as per Paxinos *et al.,* 2001) were collected using a vibratome (Pelco 101, 1000 Series) and stored in well plates in PBS until immunohistochemical staining.

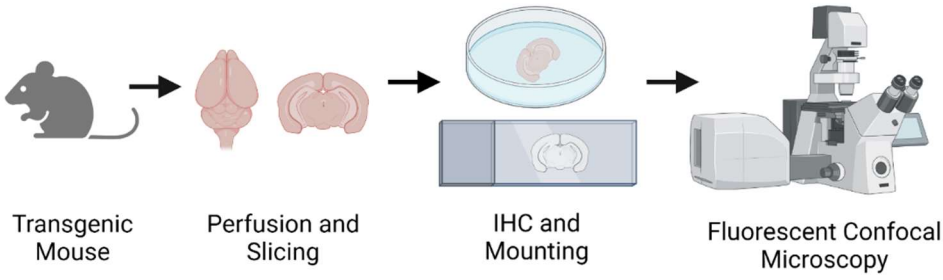

Figure 3. Methodology used to obtain confocal images for data collection. Coronal slices of DAT-Cre::ChR2-EYFP mouse brains were stained for TH and Calb through immunohistochemistry. Sections were then mounted and visualized using fluorescent confocal microscopy.

Staining took place within a week of brains being sectioned. Slices were placed in well plates and washed three times with PBS (pH 7.4) for 10 minutes. They were then permeabilized with 0.25% Triton X100 (in PBS; Bio Basic, cat# TB0198) for 10 minutes, after which they underwent three more 10-minute washes with PBS. Slices were blocked in 10% donkey serum (in PBS; Jackson ImmunoResearch, cat#017-000-121) for 30 minutes. The sections were then incubated at room temperature overnight in primary antibody (tyrosine hydroxylase, Pel Freez Biologicals, cat#P40101-150, host: rabbit; calbindin, Abcam Inc., cat#ab82812, host: mouse) in 3% donkey serum (in PBS) at a 1:250 concentration. Sections were rinsed 3 times with PBS (pH 7.4) and incubated overnight at room temperature in secondary antibodies (Alexa Fluor 405 anti-rabbit, Invitrogen, cat#ab175651, host: donkey; Cy5 anti-mouse, Jackson ImmunoResearch, cat#715-175-150) at a 1:500 concentration to 3% donkey serum. Slices were mounted with 80 µL Immunomount (Immu-Mount^{TM}, Thermo Fisher Scientific, cat# 9990402) (pH 8.0) on slides

(Superfront Plus Gold Microscope Slides, Thermo Fisher Scientific, cat# 15-188-48). The mounted slides were stored overnight at 4°C before sealing the coverslip edges with nail polish. Slides were stored at 4°C and were allowed to dry for at least 24 hours after sealing prior to imaging.

2.3 Spectral confocal microscopy

Only sections of interest in which the oculomotor nerve intersecting the SNc was clearly visible were used for imaging. A Nikon C1si scanning confocal inverted microscope was used to obtain z-stack images of regions of interest. Imaging was done at room temperature. Images for analysis were acquired using a 20X Plan Fluor DIC objective (0.50 NA, 2.1 mm working distance), and additional images were acquired using a 10X Plan Fluor DIC objective (0.30 NA, 16 mm working distance). Images were 16-bit with 1024 x 1024 pixel resolution. Cy5 was excited using a 640 nm diode laser line at 5% maximum intensity of an Obis diode laser, EYFP was excited using a 488 laser line at 5% maximum intensity of an Argon laser, and Alexa 405 was excited using a 405 nm laser line at 5-8% of an Obis diode laser. Images were averaged over 3 scans to reduce noise and taken using a medium pinhole (40 μm diameter), 5.5 μs pixel dwell time, and spectral detector gains ranging from 175-210 (Cy5, EYFP) or 190-220 (Alexa Fluor 405) inclusive. The dimensions of the Z-stacks obtained were 636.5 x 636.5 μm with a 1 μm step size over ~20-40 μm, and stacks were collected over spectral ranges of 655-705 nm (Cy5), 515-565 nm (EYFP), and 420-470 nm (Alexa Fluor 405).

2.4 Analysis of confocal microscopy images

Superimposition of z-stack images and quantification of colocalization of TH+, Calb+, and ChR2+ cells were done in Fiji (ImageJ, version 2.35/1.54t). TH+, Calb+, TH+Calb+, and TH+ChR2+ cell bodies for each region of interest were counted by hand using the cell counter feature of the Bio-Formats plugin. The medial and lateral SNc were distinguished through division by the oculomotor nerve. All cells medial to the most lateral fiber in the z-stack were included as medial during counting. The medial lemniscus served as a division between the SNc and VTA. Cells within these boundaries were included in the count for the region of interest.

Signal to background differences were measured for each fluorophore (Alexa 405, Cy5, and EYFP). Throughout each of the 27 z-stacks analyzed, 10 measures of mean pixel intensity for

each positive fluorescent signal (signal) and negative fluorescent signal (background) were collected. If there were not 10 positive cells present, all positive cells in ROI were included; in total, 270 measures were taken for each fluorophore except measures of positive Calb-Cy5 signal (267 measures taken in total). For TH-405, Calb-Cy5, and EYFP expression (respectively), the mean signal pixel intensities were 1252.19 ± 36.93, 1284.47 ± 36.93, and 780.20 ± 19.39, while the mean background intensities were 308.54 ± 11.62, 255. 35 ± 8.18, and 240.10 ± 6.50 (Fig 4). It should be noted that size, shape, and relative position throughout the z-stack was also taken into consideration when identifying cells.

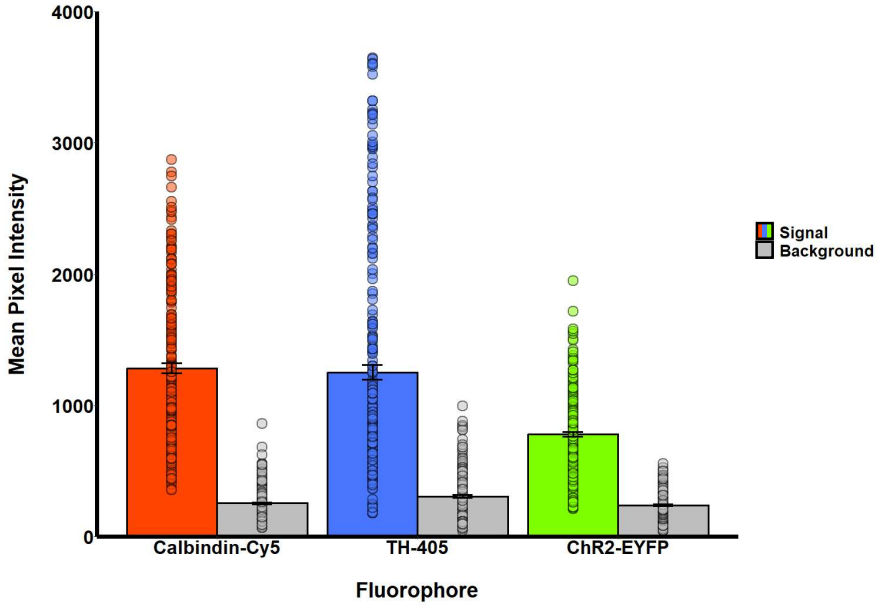

Figure 4. Mean pixel intensity of positive and negative signal for fluorophores visualized in confocal images. The mean pixel intensities of signal and background expression for the TH-405, Calb-Cy5, and ChR2-EYFP fluorophores used in the study. Measures of pixel intensity were obtained from 27 images of MSNc, LSNc, and VTA of 4 mice. The number of either signal or background measures taken per fluorophore ranged from 267-270. TH-405 expression had a mean signal pixel intensity of 1252.19 ± 36.93 and a mean background pixel intensity of 308.54 ± 11.62. Calb-Cy5 expression had a mean signal pixel intensity of 1284.47 ± 36.93 and a mean background pixel intensity of 255. 35. ChR2-EYFP expression had a mean signal pixel intensity of 780.20 ± 19.39 and a mean background pixel intensity of 240.10 ± 6.50.

2.5 Statistical analyses

Statistical analyses were carried out using R (version 4.2.2, 2022) and values were reported as mean ± standard error of the mean. The sample size used during analyses was n = 8, as data was collected from the SNc and VTA of both hemispheres of all four mice used. Assumptions of normality were tested using a Shapiro-Wilk normality test and assumptions of equal variance were tested using a Fligner-Killeen test of homogeneity of variances. When appropriate, single-factor ANOVA was used to evaluate differences between groups and was followed by a post-hoc Tukey-Kramer test for multiple comparisons of means. When parametric assumptions were not met, the Kruskal-Wallis Rank Sum test was used to detect potential differences between any groups, and if detected Dunn's test for pairwise multiple comparisons was used post-hoc to assess between which groups these differences occurred. When of interest, calculation of Cohen's d and power analyses were conducted. The alpha level of statistical significance used for all analyses was 0.05.

3.0 Results

3.1 Calb colocalization in DA neurons

To characterize the proportion of DA (TH+) neurons that co-expressed Calb within brain regions measured (Fig 6), we divided the number of neurons that were both Calb+ and TH+ by the total number of TH+ neurons present to gain a representative fraction. This was used to calculate the percentage of colocalization observed; percentages were used in statistical analyses. There was found to be a difference in the extent of TH+Calb+/TH+ colocalization between brain regions analyzed (Kruskal-Wallis rank sum test: $p < 0.001$) (Table 1). While we observed a trend in TH+Calb+/TH+ colocalization within the SNc, wherein the LSNc (6.62 ± 2.48 %) had a lower degree of colocalization than the MSNc (18.56 ± 5.49 %), this difference was not significant (Dunn's test: $p = 0.19$) (Table 1; Fig 5). Calculation of Cohen's d showed that there was a large effect size, indicating that the two true means of these regions have little overlap with each other ($d = 0.99$). A power analysis was also conducted to determine the sample size needed to have a statistical power of 0.80 given the current results of MSNc-LSNc colocalization. Results showed that a sample size of 24 would be needed to reach 95% confidence that the means were different ($\delta = 11.94$, $\alpha = 0.05$, $sd = 16.41$); this would require the use of eight more mice than in the current study. There was a strong significant difference in TH+Calb+/TH+ colocalization between the

both the MSNc and LSNc compared to the VTA (59.97 ± 3.60 %) (Dunn's test: $p = 0.01$ and $p = 1.94 \times 10^{-4}$, respectively).

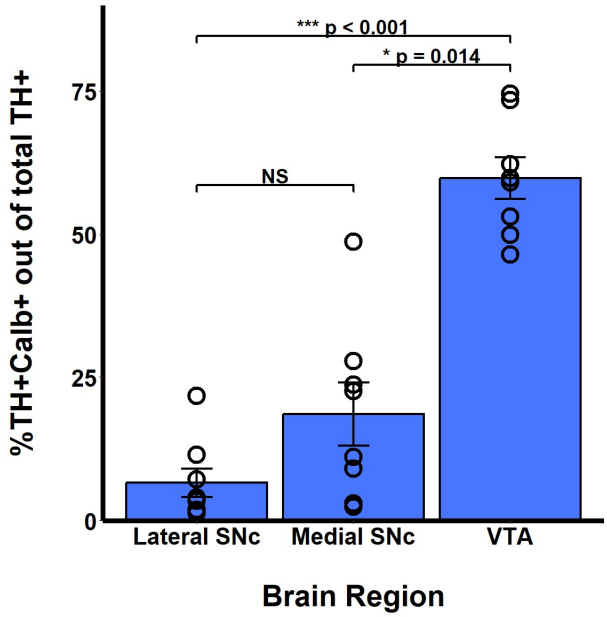

Figure 5. Percentage of Calb+ cells colocalized in DA neurons within the VTA, MSNc, and LSNc of DAT-Cre::ChR2-EFYP mice. Colocalization data was collected from a total of 27 images of the MSNc, LSNc, and VTA of both hemispheres of four mice (n = 8). There was a significantly higher degree of colocalization within the VTA (59.97 ± 3.60 %) compared to the SNc. While the mean percentage of TH+Calb+ colocalization in the MSNc (18.56 ± 5.49) was higher than that of the LSNc (6.62 ± 2.48), the difference between them was not significant.

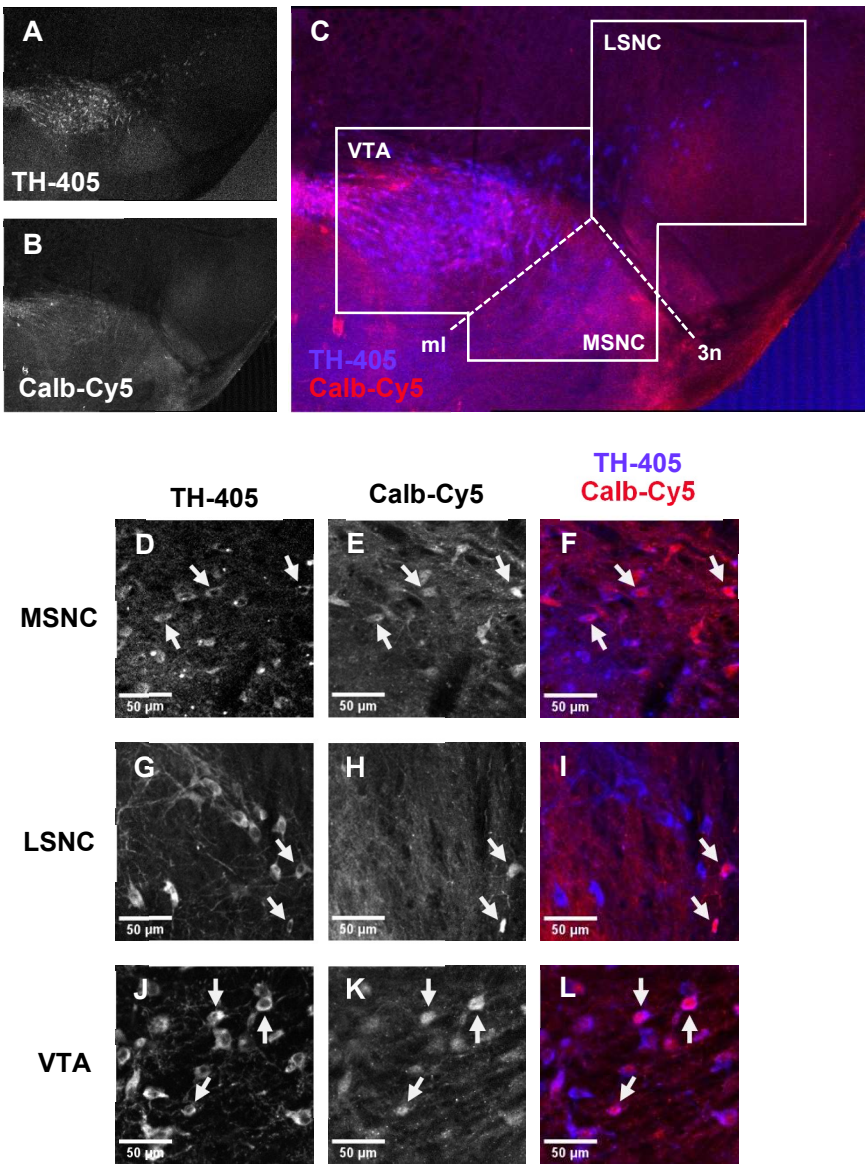

Figure 6. Colocalization of Calb and TH in the dopaminergic midbrain of DAT-Cre:ChR2-EYFP mice. 10X confocal images of the dopaminergic (TH+) and Calb+ mouse midbrain are shown in **A** and **B** (respectively). These images are superimposed in **C** to show regions of interest. The MSNc and LSNc were divided by the oculomotor nerve (3n), while the MSNc and VTA were separated by the medial lemniscus (ml). Cell counting was performed using 20X confocal images (**D-L**). The TH+, Calb+, and superimposed images are shown for the MSNc (**D-F**), LSNc (**G-I**), and VTA (**J-L**). Colocalizing TH+Calb+ neurons in each region of interest are shown by the arrows in each panel. Data for each brain region consisted of counts from a total of 27 images of the MSNc, LSNc, and VTA in both hemispheres of from four mice (n = 8).

3.2 Proportion of Calb+ cells that are DA

The percentage of Calb+ neurons that were DA (TH+) was deduced using the same method as section 3.2, except now dividing the number of TH+Calb+ neurons by the total number of Calb+ neurons present in the region of interest (Fig 6). The mean percentages of TH+Calb+/Calb+ colocalization were 26.47 ± 6.80% (LSNc), 34.47 ± 4.59% (MSNc), and 42.31 ± 5.41% (VTA) (Table 1). Single-factor ANOVA found no significant differences between either of these brain regions (p = 0.17) (Fig 7A). These results indicate that while the proportion of total DA neurons expressing Calb may differ between brain regions, the proportion of Calb devoted to the DA cell population remains the same between all brain regions.

The presence of non-DA Calb+ positive cells is also informative when characterizing the pattern of Calb+ throughout the midbrain. The percent of TH+Calb+/Calb+ colocalization not only conveys the relative amount of Calb+ cells that are DA but can also be used to infer the proportion of Calb+ cells present in these regions that belong to other neurotransmitter systems or have a supportive function (Fig 7B). Using 1 - TH+Calb+/Calb+, the percentage of non-DA Calb+ cells in the LSNc, MSNc, and VTA are calculated to be 73.53± 6.80%, 65.53± 4.59%, and 57.69± 5.41% respectively.

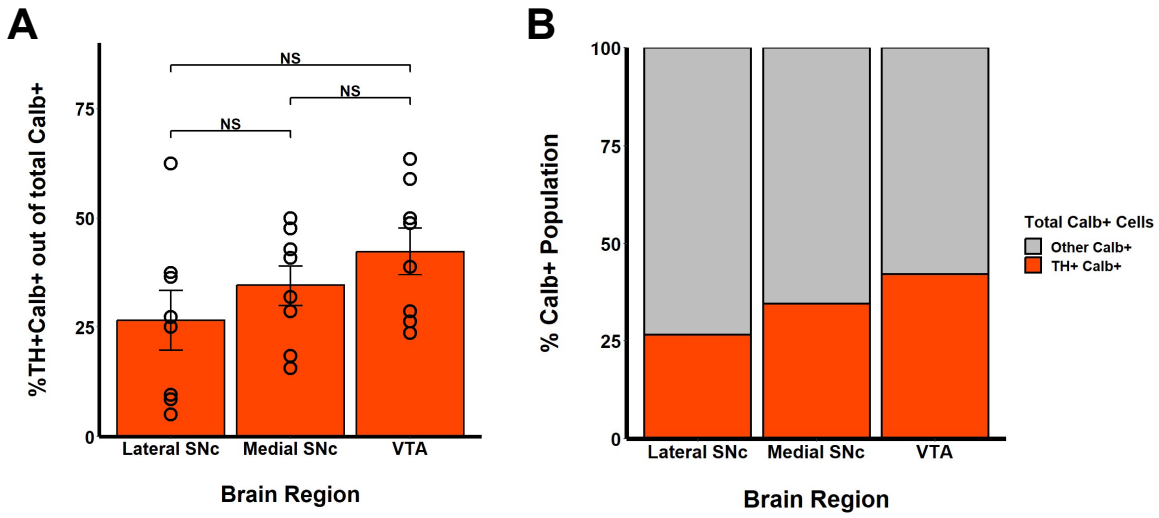

Figure 7. Percentage of TH+ colocalized in Calb+ neurons within the VTA, MSNc, and LSNc of DAT-Cre::ChR2-EFYP mice. Colocalization data was collected from a total of 27 images of the MSNc, LSNc, and VTA of both hemispheres of four mice (n = 8). As shown by **A,** there was no difference in colocalization between the VTA (42.31 ± 5.41 %), MSNc (34.47±4.59 %), or LSNc (26.47±6.80%) (Single-factor ANOVA: p = 0.17). The stacked bar chart shown in **B** depicts how much of the Calb+ population in each brain region is devoted to DA neurons and how much are non-DA cells.

3.3 ChR2 expression within DA neurons

Percentages of ChR2 expression in DA neurons within regions of interest were calculated in the same manner as section 3.2, but now with the number of TH+ChR2 colocalized neurons (Fig 9). Levels of TH+ChR2+/TH+ colocalization was observed to be very high within all regions analyzed; in DA neurons, the LSNc, MSNc, and VTA had ChR2+ colocalization levels of 98.33 ± 0.64%, 96.89 ± 0.63%, and 95.73 ± 0.77% respectively (Table 1; Fig 8). Due to the observed closeness of means and low variability within the samples, we did not perform statistical analyses to compare colocalization levels between brain regions. These results suggest that the DAT-Cre::ChR2-EYFP mouse model is very effective at expressing ChR2 in the DA neurons within these regions. It should be noted that these results do not convey any information about ChR2 expression outside of DA neurons.

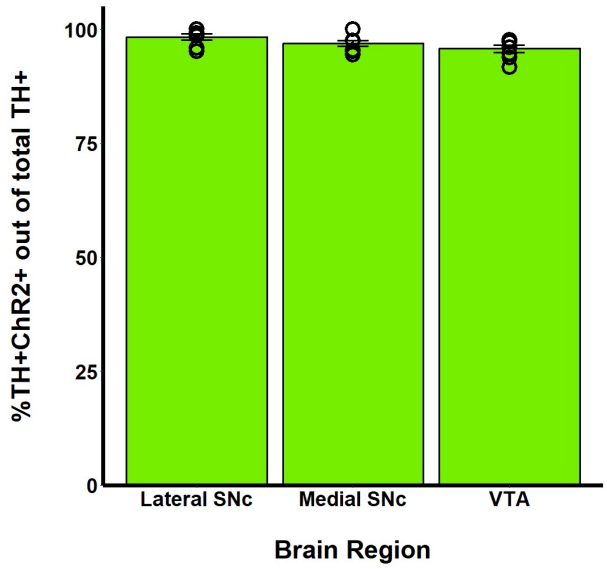

Figure 8. Percentage of TH+ChR2+ colocalization in DA neurons within the VTA, MSNc, and LSNc of DAT-Cre::ChR2-EFYP mice. Colocalization data was collected from a total of 27 images of the MSNc, LSNc, and VTA of both hemispheres of four mice (n = 8). Expression of ChR2 was extremely high in midbrain DA neurons, with the VTA, LSNc, and MSNc having mean percentages of ChR2+TH+ colocalization of 95 ± 0.77 %, 98.33 ± 0.64 %, and 96.89 ± 0.63 % (respectively).

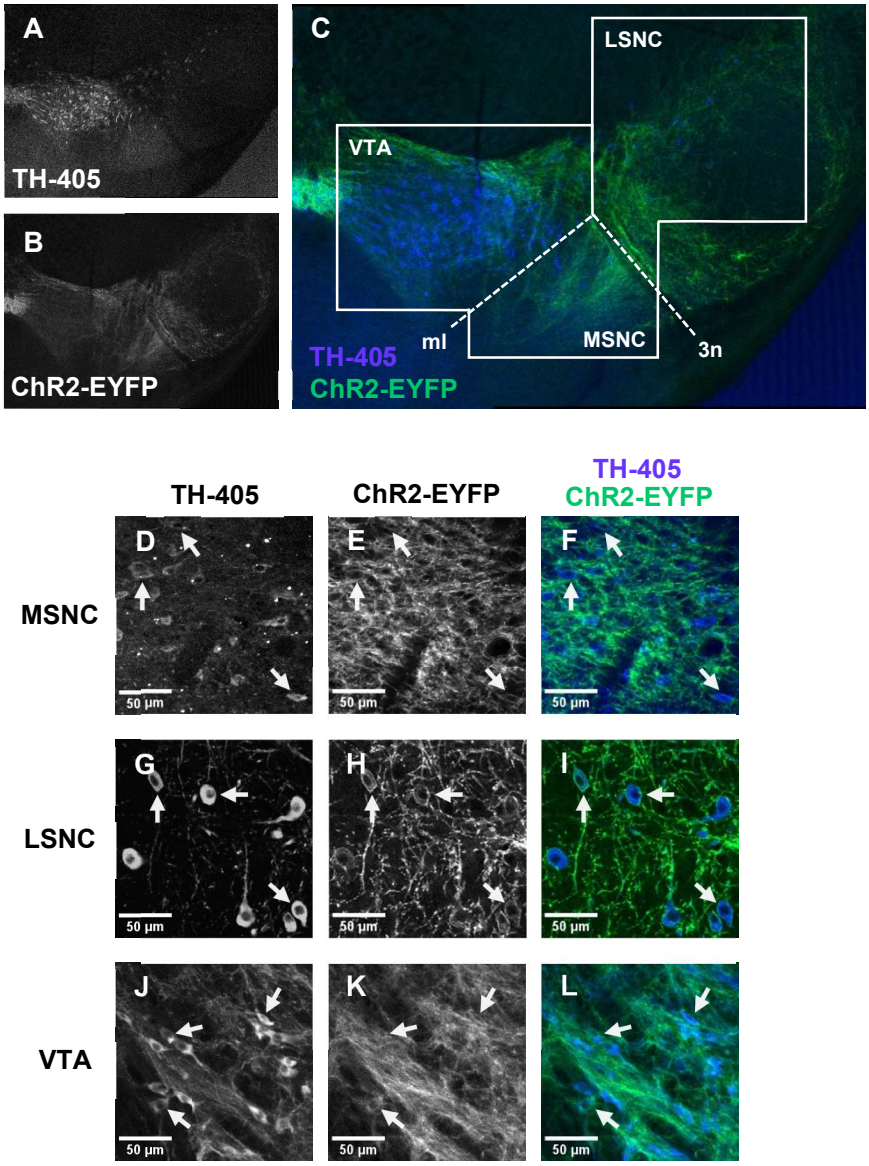

Figure 9. Colocalization of ChR2 and TH in the dopaminergic midbrain of DAT-Cre:ChR2-EYFP mice. 10X confocal images of the dopaminergic (TH+) (**A**) and ChR2+ (**B**) mouse midbrain were obtained for cell counting. **C** depicts a superimposition of both ChR2+ and TH+ images and denotes the regions of interest used when quantifying colocalization. The oculomotor nerve (3n) was used to divide the medial and lateral SNc, and the medial lemniscus (ml) was used to separate the MSNc with the VTA. Cell counting was performed using 20X confocal images (**D-L**). The TH+, ChR2+, and superimposed images are shown for the MSNc (**D-F**), LSNc (**G-I**), and VTA (**J-L**). Arrows highlight colocalized TH+ChR2+ neurons in each region of interest. Data for each brain region consisted of counts from a total of 27 images of the MSNc, LSNc, and VTA of both hemispheres of from four mice (n = 8).

3.4 Calb-reactive neurites and neuropil in the SN

During our analysis, we observed robust Calb+ staining of the neuropil in the SNc and the dorsolateral region of the SNR of all brains (Fig 10A, Fig 10B). There were also neurite-like structures that appeared throughout the entire mediolateral axis of the SNR (Fig 10C, Fig 10D) and SNc. As our TH stain appeared to be solely localized to the somas of DA neurons, we are unable to determine if DA processes colocalize with these structures. These results show that structures other than cells bodies are Calb+ in the SN.

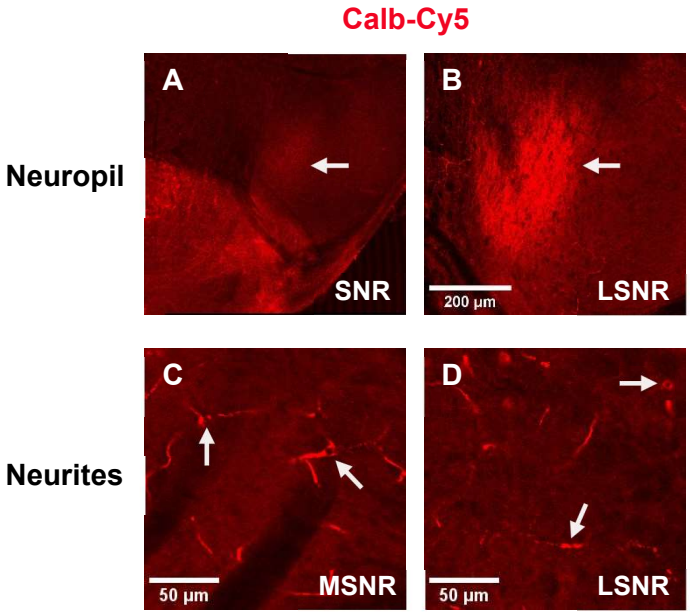

Figure 10. Calb+ reactivity of neuropil and non-somatic structures in the SNR of the DAT-Cre::ChR2-EYFP mouse midbrain. Neuropil in the dorsolateral SNR showed intense reactivity to immunostaining for Calb; this can be seen in 10X images (**A**) but is even more apparent in 20X images (**B**). **C** and **D** show the presence of neurite-like structures present within both the medial and lateral SNR.

4.0 Discussion

4.1 Calb expression in DA neurons does not differ between the LSNc and MSNc

The relative distribution of Calb in DA neurons has been debated in the scientific literature. While the current study observed a trend similar to that of Nemoto *et al.* (1999) and others, in which the MSNc had a larger mean percentage of Calb+ colocalization in DA neurons than the LSNc, this difference was not statistically significant. Past studies conducting similar colocalization studies in rats have found significant effects with sample sizes ranging from 3-6 (Liang *et al.,* 1996; Nemoto *et al.,* 1999; Rogers and Résibois, 1992). That said, it is likely that the non-significance between the MSNc and LSNc in their degree of TH+Calb+/TH+ colocalization is not due to our sample size being too small. Therefore, these results show that while the VTA shows a much higher percentage of DA neurons with TH+/Calb+ colocalization the percentage of this colocalization is likely the same between the medial and lateral SNc. However, the limitations of the study must be acknowledged when considering this result.

One potential drawback may have been that data was only collected from one section per mouse. McRitchie and Halliday (1995) observed the presence of Calb+ DA cells in the medial SNc of humans but noted that the population was very small and caudally localized. Liang *et al.* (1996) investigated the expression of Calb+ throughout the SNc along the entire rostrocaudal axis and found that only 20% of the SNc DA neurons contain Calb. Taking into consideration the small amount of Calb+ cells within the SNc and this observed heterogeneity along the rostrocaudal axis, analyzing one section per animal may have not allowed for a fully comprehensive view of these cells within the SNc even if more animals were used. Furthermore, although comparisons were made between colocalization percentages, only analyzing one section may have also reduced the "cellular sample size"; for example, sometimes the LSNc contained a large enough number of DA neurons that two image stacks needed to be analyzed during data collection for the region, while other times data collection only required one stack. The MSNc, on the other hand, sometimes contained very few DA neurons, with the presence of even one TH+Calb+ cell influencing the percentage of colocalization substantially and contributing to the variability seen in our data. While other investigative studies had a similar subject sample size to the present study, most tend to analyze multiple sections per subject (Dopeso-Reyes, 2014; Nair-Roberts *et al.,* 2008). That said,

the analysis of additional sections from each mouse may have allowed our data to more accurately reflect any Calb-related trends that occur within the SNc.

While there was no difference in the percentage of TH+Calb+ colocalization within the SNc itself, there were large significant differences found between both the MSNc and LSNc and the VTA. This is in accordance with past research showing higher levels of Calb in the VTA as compared to the SNc, which suggests that the Dat-Cre::ChR2-EYFP mouse model examined displays typical patterns of Calb expression (Damier *et al.,* 1999; Dopeso-Reyes, 2014; Liang *et al.,* 1996).

4.2 Other potential markers for physiological differences between midbrain regions

While we suspect that variability within the SNc may be the reason for the non-significance of the medial/lateral difference in DA Calb expression in the SNc, other potential markers for the physiological differences that have been observed between the medial and lateral DA SNc should be considered. Chung *et al.* (2005) aimed to uncover physiological markers that differed between the DA neurons in the SNc and VTA. Among markers they identified were GIRK channels and cholecystokinin (CCK).

One potential marker that could be considered is expression of G-protein-regulated inward-rectifier potassium 2 (GIRK2) channels. Gain-of-function of GIRK2 has been shown to potentially alter the electrophysiological phenotype of DA neurons through activation of K-ATP channels (Liss *et al.,* 1999). Therefore, perhaps the physiological heterogeneity in the DA midbrain is not due to Calb's influence on K-ATP channels but through the influence of GIRK2. Interestingly, Calb+ and GIRK2 colocalization in DA neurons has been found to be higher in the lateral SNc than the medial, while overall Calb expression is higher in the MSNc than the LSNc (Reyes *et al.,* 2012). Additionally, GIRK2+ DA neurons have been associated with increased vulnerability to Parkinsonian-like cell death, in contrast to Calb+ DA neurons as previously described (Chung *et al.,* 2005). Therefore, perhaps it is both Calb expression and GIRK2 expression that contribute to relative differences in vulnerability to cell death within the DA midbrain.

There are also increased levels of the neuropeptide cholecystokinin (CCK) in the VTA relative to the SNc (Chung *et al.,* 2005). In the DA neurons of the VTA, CCK acts to regulate the

excitability of these DA neurons by facilitating long-term potentiation of GABAergic synapses upon release (Martinez Damonte *et al.,* 2023). It has also been shown to have neuroprotective effects on DA neurons in the substantia nigra through decreasing neuroinflammation and mitochondrial damage (Zhang *et al.,* 2022). One study characterized CCK as colocalizing with DA neurons in the medial SNc, which would correlate with the resilience of this region to cell death (Hommer *et al.,* 1985). Therefore, more current research should be done to establish CCK's pattern of expression within the SNc itself, in addition to characterizing if its presence effects the excitability of DA neurons in a similar manner as in the VTA.

Other genes that were elevated in the SNc include those related to metabolism, mitochondrial proteins, and lipid, protein, and vesicle-mediated transport (Chung *et al.,* 2008). Therefore, while Calb is a strong potential marker for distinct physiological characteristics in DA neurons, research on expression patterns of other markers and their ability to modulate DA neurotransmission could be valuable in establishing a complete understanding of the observed physiological heterogeneity within the DA midbrain.

4.3 Not all Calb present in the midbrain is devoted to DA neurons

The percentage of the total Calb+ cells present that were colocalized with TH remained constant between the MSNc, LSNc, and VTA. While there were no differences between brain regions, the mean percentage of this colocalization for all brain regions was less than half of the total Calb+ population present. That said, there remains a substantial amount of Calb+ cells in these regions that are not involved in the DA system, which poses the question of what cell types make up this additional Calb+ population.

One possibility is that these cells are GABAergic neurons. One stereological study by Nair-Roberts *et al.* observed that 29% of cells in the SNc and 35% of VTA cells were both GABAergic and non-DA. Within the SNc, these cells tend to be located laterally (Nair-Roberts *et al.,* 2008). However, it has been found that only a very small amount of non-DA GABAergic neurons in the VTA colocalize with Calb (Olson and Nestler, 2007). To the best of our knowledge, the extent of GABA+Calb+ colocalization within the SNc has yet to be quantified. It has been observed that in GABAergic neurons, Calb may play a role in slowing the extent of Ca^{2+} increase in response to

oxidative and glucogenic deprivation induced by domoic acid exposure (Zinchenko *et al.,* 2021). Therefore, Calb may play a neuroprotective role in GABAergic neurons in addition to DA neurons. Investigating the potential presence of Calb+ GABAergic neurons within the SNc and VTA would be worthwhile, especially as a loss in GABAergic transmission has recently been theorized to contribute to abnormal calcium levels leading to neurodegeneration in various diseases (Blaszczyk, 2016).

Glutamatergic neurons could also make up part of the Calb+ population we observed in the midbrain. The VTA contains a small glutamatergic neuronal population that is distinct from both GABAergic and DA populations (Nair-Roberts *et al.,* 2008; Yamaguchi, Sheen, and Morales, 2011). The presence of glutamatergic neurons within the SNc has been much more debated, but more recent research shows that the lateral SNc does contain discretely glutamatergic neurons expressing VGLUT-2 (An *et al.,* 2021; Root *et al.,* 2016; Yamaguchi *et al.,* 2013). While studies on Calb expression within these glutamatergic SNc neurons are lacking, Mongia *et al.* (2020) demonstrated that roughly one-third of glutamatergic neurons in the VTA expressed Calb. In the VTA, glutamatergic neurons are known to modulate behaviour, reinforcement learning and wakefulness (Barbano *et al.,* 2020; Root *et al.,* 2016; Yu *et al.,* 2019; Zell *et al.,* 2020). Glutamatergic SNc neurons are hypothesized to have a similar function (Root *et al.,* 2016), but studies that directly examine the function of these specific neurons have yet to be conducted. Furthermore, to the best of our knowledge there are no studies investigating if Calb+ glutamatergic neurons present in the midbrain have distinct functional or physiological characteristics. Therefore, it is possible that these Calb+ neurons could represent a unique subset of the glutamatergic population.

Our study showed that a significantly large proportion of Calb present in the midbrain is localized to neurons other than the DA neurons investigated here. Thus, studies to decipher what systems these Calb+ cells belong to could help provide a more holistic understanding of the different cell populations (and subpopulations) within the VTA and SNc.

4.4 The DAT-Cre::ChR2-EYFP model is effective in expressing ChR2 in DA neurons

ChR2 has emerged as a useful optogenetic tool that can be used in conjunction with the Cre-lox system to selectively activate certain cell types and regions (Bäckman *et al.,* 2004; Madisen *et al.,* 2012). The effects of this activity can then be observed to help elucidate the functionality of different neuronal cell types or regions within the nervous system. The DAT-Cre mouse model allows the DA system to be targeted through conditional expression of ChR2 in DA neurons. In all three midbrain regions of interest we observed, there was very high levels of ChR2 expression within DA neurons. This validates the DAT-Cre::ChR2-EYFP mouse model in its ability to harness the Cre/lox system to drive expression of ChR2 in DA neurons. However, this is only one facet of this model's evaluation. Another important aspect that should be considered is the potential for "leaky" cre recombinase. This occurs when there is ectopic cre recombinase expression, which in this case would involve cre expression outside of DAT-expressing neurons. If this occurs, then ChR2 would be expressed in non-DA neurons, and therefore may contribute to any effect observed from light stimulation. Furthermore, transgenics homozygous for the ChR2 transgene such as those investigated in this study have been reported to have a low level of "off-target" transgene expression in which ChR2-EYFP is expressed independent of cre expression (Prabhakar *et al.,* 2019). That said, the natural next step in evaluating the efficacy of the DAT-cre::ChR2-EYFP model would be to quantify the degree of non-DA ChR2 expression that occurs, either due to ectopic cre expression or Cre-independent transgene expression. While our results show that this model expresses ChR2 in DA neurons very efficiently, this finding would carry far less weight should it be revealed that ChR2 is expressed in many other non-DA neurons. Verifying a high degree of DA-localized ChR2 expression would solidify the DAT-Cre:ChR2-EYFP mouse model as a highly effectual tool for investigating the activity of the DA system.

4.5 Hypothesized identification of Calb-reactive neuropil and structures in the SNR

Damier *et al.* (1999) observed similar patterns of Calb immunoreactivity in the neuropil of the substantia nigra, similar to the intense Calb+ staining in the dorsolateral SNR observed in the current study. Authors theorized that this neuropil makes up fibers from MSNs of the direct basal ganglia pathway, which project from the striatum and synapse onto GABAergic neurons in the SNR (Damier *et al.,* 1999; Gerfen, 1984). MSNs that reside in the striatal matrix are known to be

Calb+, while those that reside in striatal striosomes are Calb- (Liu and Graybiel, 1992). While MSNs that project to the SNR can originate in both the matrix and striosome compartments, the bulk of these neurons reside in the Calb+ matrix (Fujiyama *et al.,* 2011; Smith *et al.,* 2016; Watabe-Uchida *et al.,* 2012). Therefore, the neuropil and neurite-like structures in the current study could be MSN projections from the striatal matrix onto GABAergic neurons in the SNR. The subsequent projections of these SNR GABAergic neurons onto DA neurons in the SNc may also contribute to this observed Calb reactivity (Damier *et al.,* 1999; Tepper *et al.,* 1995)

Alternatively, these structures may be microglia. Microglia function to support and protect neurons and are known to be particularly abundant within the substantia nigra, especially in the SNR (Lawson, Perry, and Gordon, 1990). Microglia within the SNc become activated by alpha-synuclein during Parkinson's disease and induce neuroinflammation which contributes to the DA cell death characteristic of the disease (Tanaka *et al.,* 2013). While there is a lack of knowledge in the field surrounding Calb expression in microglia, the calcium-binding protein Iba1 is known to be specifically expressed in microglia and influences the functioning of activated microglia (Ito *et al.,* 1998). Calb may function in a similar manner. The exact role Calb plays in microglial functioning is a potential subject for future research.

4.6 Future research

As the role of Calb as a physiological marker remains ambiguous, further studies to characterize Calb colocalization within DA neurons along the mediolateral SNc should be conducted. These studies should be sure to acknowledge heterogeneity in Calb expression along other axes, as well as take into consideration the small number and caudal localization of Calb+ DA neurons within the SNc (Liang *et al.,* 1996; McRitchie and Halliday, 1995). Future studies should investigate if the non-DA Calb+ midbrain neurons we have described here make up functionally distinct subpopulations. It would also be useful to know the relative expression of these subpopulations along different axes of the midbrain should they be applicable to any observed physiological differences between axes. The validity of the DAT-Cre::ChR2-EYFP mouse model could be further strengthened if it was shown that there were low levels of ectopic cre or ChR2 expression outside of DA neurons. The extent of leaky cre expression of the DAT-Cre::ChR2-EYFP mouse line could be quantified through performing a Hoechst stain combined with labelling for TH so

that ChR2 expressed in non-DA neurons could be identified. Finally, research confirming the hypothesized presence of Calb in microglia within the substantia nigra, and the role it may play in microglial functioning might also be of future interest.

5.0 Conclusion

This study provided more insight into Calb colocalization in DA midbrain neurons and found that while TH+Calb+ colocalization was higher in the VTA than SNc, there was no significant difference in TH+Calb+ colocalization between the MSNc and LSNc. The possible presence of Calb+ subpopulations of other neuronal cell types present in the midbrain was also discussed. We also, to the best of our knowledge, conducted a novel attempt in evaluating the efficacy of the DAT-Cre::ChR2-EYFP mouse model and reported an extremely high ability of this mouse line to express ChR2 in DA cells. This research may have important implications in understanding molecular and physiological heterogeneity within the midbrain, as well as providing useful information for future studies that will utilize the DAT-Cre::ChR2-EYFP mouse model.

6.0 References

Adcock, R. A., Thangavel, A., Whitfield-Gabrieli, S., Knutson, B., & Gabrieli, J. D. (2006). Reward-motivated learning: mesolimbic activation precedes memory formation. *Neuron, 50*(3), 507–517. https://doi.org/10.1016/j.neuron.2006.03.036

Alberico, S. L., Cassell, M. D., & Naraynan, N. S. (2015). The vulnerable ventral tegmental area in Parkinson's disease. *Basal Ganglia, 5*(2-3), 51-55. https://doi.org/10.1016/j.baga.2015.06.001

Alilain, W. J., Li, X., Horn, K. P., Dhingra, R., Dick, T. E., Herlitze, S., & Silver, J. (2008). Light-induced rescue of breathing after spinal cord injury. *The Journal of Neuroscience, 28*(46), 11862–11870. https://doi.org/10.1523/JNEUROSCI.3378-08.2008

An, S., Li, X., Deng, L., Zhao, P., Ding, Z., Han, Y., Luo, Y., Liu, X., Li, A., Luo, Q., Feng, Z., & Gong, H. (2021). A whole-brain connectivity map of VTA and SNc glutamatergic and GABAergic neurons in mice. *Frontiers in Neuroanatomy, 15.* https://doi.org/10.3389/fnana.2021.818242

Anderegg, A., Poulin, J. F., and Awatramani, R. (2016). Molecular heterogeneity of midbrain dopaminergic neurons – moving toward single cell resolution. *FEBS Letters, 589*(24). https://doi.org/10.1016%2Fj.febslet.2015.10.022

Bäckman, C. M., Malik, N., Zhang, Y., Shan, L., Grinberg, A., Hoffer, B. J., Westphal, H. & Tomac, A. C. (2006). Characterization of a mouse strain expressing cre recombinase from the 3' untranslated region of the dopamine transporter locus. *Genesis, 44*(8), 383-390.

Badgaiyan R. D. (2010). Dopamine is released in the striatum during human emotional processing. *Neuroreport, 21*(18), 1172–1176. https://doi.org/10.1097/WNR.0b013e3283410955

Barbano, M. F., Wang, H. L., Zhang, S., Miranda-Barrientos, J., Estrin, D. J., Figueroa-González, A., Liu, B., Barker, D. J., & Morales, M. (2020). VTA Glutamatergic Neurons Mediate Innate Defensive Behaviors. *Neuron*, *107*(2), 368–382.e8. https://doi.org/10.1016/j.neuron.2020.04.024

Bernheimer, H., Birkmayer, W., Hornykiewicz, O., Jellinger, K., & Seitelberger, F. (1973). Brain dopamine and the syndromes of Parkinson and Huntington. Clinical, morphological and neurochemical correlations. *Journal of the Neurological Sciences, 20*(4), 415–455. https://doi.org/10.1016/0022-510x(73)90175-5

Best, J. A., Nijhout, H. F., & Reed, M. C. (2009). Homeostatic mechanisms in dopamine synthesis and release: a mathematical model. *Theoretical biology & medical modelling*, *6*(21). https://doi.org/10.1186/1742-4682-6-21

Bi, A., Cui, J., Ma, Y. P., Olshevskaya, E., Pu, M., Dizhoor, A. M., & Pan, Z. H. (2006). Ectopic expression of a microbial-type rhodopsin restores visual responses in mice with

photoreceptor degeneration. *Neuron, 50*(1), 22-33. https://doi.org/10.1016/j.neuron.2006.02.026

Blaszczyk J. W. (2016). Parkinson's Disease and Neurodegeneration: GABA-Collapse Hypothesis. *Frontiers in neuroscience*, *10*, 269. https://doi.org/10.3389/fnins.2016.00269

Boyden, E. S., Zhang, F., Bamberg, E., Nagel, G., and Deisseroth, K. (2005). Millisecond-timsescale, genetically target optical control of neural activity. *Nature Neuroscience, 8*, 1263-1268.

Brimblecombe, K. R., Vietti-Michelina, S., Platt, N. J., Kastli, R., Hnieno, A., Gracie, C. J., & Cragg, S. (2019). Calbindin-D28k limits dopamine release in ventral but not dorsal striatum by regulating Ca^{2+} availability and dopamine transporter function. *ACS Chemical Neuroscience, 10*(8), 3419-3426.

Britt, J. P., McDevitt, R. A., & Bonci, A. (2012). Use of channelrhodopsin for activation of CNS neurons. *Current protocols in neuroscience, 2*(2). https://doi.org/10.1002/0471142301.ns0216s58

Calì, T., Ottolini, D., Negro, A., & Brini, M. (2012). α-Synuclein controls mitochondrial calcium homeostasis by enhancing endoplasmic reticulum-mitochondria interactions. *The Journal of biological chemistry*, *287*(22), 17914–17929. https://doi.org/10.1074/jbc.M111.302794

Carlsson, A., Lindqvist, M., & Magnusson, T. (1957). 3,4-Dihydroxyphenylalanine and 5-hydroxytryptophan as reserpine antagonists. *Nature, 180*(4596), 1200. https://doi.org/10.1038/1801200a0

Chard, P. S., Bleakman, D., Christakos, S., Fullmer, C. S., & Miller, R. J. (1993). Calcium buffering properties of calbindin D28k and parvalbumin in rat sensory neurones. *The Journal of Physiology*, *472*, 341–357. https://doi.org/10.1113/jphysiol.1993.sp019950

Chard, P. S., Bleakman, D., Christakos, S., Fullmer, C. S., & Miller, R. J. (1993). Calcium buffering properties of calbindin D28k and parvalbumin in rat sensory neurones. *The Journal of physiology*, *472*, 341–357. https://doi.org/10.1113/jphysiol.1993.sp019950

Christakos, S., & Liu, Y. (2004). Biological actions and mechanism of action of calbindin in the process of apoptosis. *The Journal of Steroid Biochemistry and Molecular Biology, 89*(90), 401-404. https://doi.org/10.1016/j.jsbmb.2004.03.007

Chung, C. Y., Seo, H., Sonntag, Brooks, A., Lin, L., Isacson, O. (2005). Cell type-specific gene expression of midbrain dopaminergic neurons reveal molecules involved in their vulnerability and protection. *Human Molecular Genetics, 14*(13), 1709-1725.

Damier, P., Hirsch, E. C., Agid, Y., & Graybiel, A. M. (1999). The substantia nigra of the human brain. I. Nigrosomes and the nigral matrix, a compartmental organization based on calbindin D(28K) immunohistochemistry. *Brain : a journal of neurology*, *122 (Pt 8)*, 1421–1436. https://doi.org/10.1093/brain/122.8.1421

Dang, L. C., O'Neil, J. P., & Jagust, W. J. (2012). Dopamine supports coupling of attention-related networks. The Journal of neuroscience : the official journal of the Society for *Neuroscience, 32*(28), 9582–9587. https://doi.org/10.1523/JNEUROSCI.0909-12.2012

Dopeso-Reyes, I., Rico, A. J., Roda, E., Sierra, S., Pignataro, D., Lanz, M., Sucunza, D., Change-Azancot, L., & Lanciego, J. L. (2014). Calbindin content and differential vulnerability of midbrain efferent dopaminergic neurons in macaques. *Frontiers in Neuroanatomy, 8*(146). https://doi.org/10.3389/fnana.2014.00146

Ehringer, H., & Hornykiewicz, O. (1998). Distribution of noradrenaline and dopamine (3-hydroxytyramine) in the human brain and their behavior in diseases of the extrapyramidal system. *Parkinsonism & Related Disorders, 4*(2), 53–57. https://doi.org/10.1016/s1353-8020(98)00012-1

Estakhr, J., Abazari, D., Frisby, K., McIntosh, J. M., & Nashmi, R. (2017). Differential control of dopaminergic excitability and locomotion by cholinergic inputs in mouse substantia nigra. *Current Biology, 27*(13), 1900-1914. https://doi.org/10.1016/j.cub.2017.05.084

Evans, R. C., Zhu, M., & Khaliq, Z. M. (2017). Dopamine inhibition differentially controls excitability of substantia nigra dopamine neuron subpopulation through T-Type calcium channels. *Journal of Neuroscience, 37*(13), 3704-3720. https://doi.org/10.1523/jneurosci.0117-17.2017

Everitt, B. J., Morris, K. A., O'Brien, A., & Robbins, T. W. (1991). The basolateral amygdala-ventral striatal system and conditioned place preference: further evidence of limbic-striatal interactions underlying reward-related processes. *Neuroscience*, *42*(1), 1–18. https://doi.org/10.1016/0306-4522(91)90145-e

Fearnley, J. M., & Lees, A. J. (1991). Ageing and parkinson's disease: substantia nigra regional selectivity. *Brain, 114*(5), 2283-2301. https://doi.org/10.1093/brain/114.5.2283

François, C., Yelnik, J., Tandé, D., Agid, Y., & Hirsch, E. C. (1999). Dopaminergic cell group A8 in the monkey: anatomical organization and projections to the striatum. *The Journal of comparative neurology*, *414*(3), 334–347.

Franklin, K. B. J, & Wolfe, J. (1987). Opposed locomotor asymmetries following lesions of the medial and lateral substantia nigra pars compacta or pars reticulata in the rat. *Physiology and Behaviour, 40*(6), 741-745. https://doi.org/10.1016/0031-9384(87)90277-0

Fu, Y., Yuan, Y., Halliday, G., Rusznák, Z., Watson, C., & Paxinos, G. (2011). A cytoarchitectonic and chemoarchitectonic analysis of the dopamine cell groups in the substantia nigra, ventral tegmental area, and retrorubral field in the mouse. *Brain Structure and Function, 217*, 591-612.

Fujiyama, F., Sohn, J., Nakano, T., Furuta, T., Nakamura, K. C., Matsuda, W., & Kaneko, T. (2011). Exclusive and common targets of neostriatofugal projections of rat striosome neurons: A single neuron-tracing study using a viral vector. *European Journal of Neuroscience, 33*(4), 668–677. https://doi.org/10.1111/j.1460-9568.2010.07564.x

Garau, L., Govoni, S., Stefanini, E., Trabucchi, M., & Spano, P. F. (1978). Dopamine receptors: pharmacological and anatomic evidences indicate that two distinct dopamine receptor population are present in rat striatum. *Life Sciences, 23*(17-18), 1745-1750. https://doi.org/10.1016/0024-3205(78)90102-9

Gerfen C. R. (1984). The neostriatal mosaic: compartmentalization of corticostriatal input and striatonigral output systems. *Nature, 311*(5985), 461–464. https://doi.org/10.1038/311461a0

Gerfen, C. R., Baimbridge, K. G., & Thibault, J. (1987). The neostriatal mosaic: III. Biochemical and developmental dissociation of patch-matrix mesostriatal system. *Journal of Neuroscience, 7*(12), 3935-3944. https://doi-org.ezproxy.library.uvic.ca/10.1523/JNEUROSCI.07-12-03935.1987

Gerfen, C. R., Engber, T. M., Mahan, L. C., Susel, Z., Chase, T. N., Monsma, F. J., & Siblet, D. R. (1990). D1 and D2 dopamine receptor-regulated gene expression of striatonigral and striatopallidal neurons. *Science, 250*(4986), 1429-1432. https://doi.org/10.1126/science.2147780

Gibb, W. R., & Lees, A. J. (1991). Anatomy, pigmentation, ventral and dorsal subpopulations of the substantia nigra, and differential cell death in Parkinson's disease. *Journal of Neurology, Neurosurgery, and Psychiatry, 54*(5), 388–396. https://doi.org/10.1136/jnnp.54.5.388

Gompf, H. S., Budygin, E. A., Fuller, P. M., & Bass, C. E. (2015). Targeted genetic manipulations of neuronal subtypes using promoter-specific combinatorial AAVs in wild-type animals. *Frontiers in behavioral neuroscience*, *9*, 152. https://doi.org/10.3389/fnbeh.2015.00152

Gribb, W. R. G., & Lees, A. J. (1991). Anatomy, pigmentation, ventral and dorsal subpopulations of the substantia nigra, and differential cell death in Parkinson's disease. *Journal of Neurology, Neurosurgery, and Psychiatry, 54,* 388-396.

Gurevich, V. V., & Benovic, J. L. (1993). Visual arrestin interaction with rhodopsin. Sequential multisite binding ensures strict selectivity toward light-activated phosphorylated rhodopsin. *The Journal of biological chemistry*, *268*(16), 11628–11638.

Haber, S. N. (2014). The place of dopamine in the cortico-basal ganglia circuit. *Neuroscience, 282*, 248-257. https://doi.org/10.1016/j.neuroscience.2014.10.008

Harz, H., Hegemann, P. (1991). Rhodopsin-regulated calcium currents in *Chlamydomonas*. *Nature, 351*, 489–491. https://doi.org/10.1038/351489a0

Hight, A. E., Kozin, E. D., Darrow, K., Lehmann, A., Boyden, E., Brown, M. C., & Lee, D. J. (2015). Superior temporal resolution of Chronos versus channelrhodopsin-2 in an optogenetic model of the auditory brainstem implant. Hearing research, 322, 235–241. https://doi.org/10.1016/j.heares.2015.01.004

Hommer, D. W., Palkovits, M., Crawley, J. N., Paul, S. M., & Skirboll, L. R. (1985). Cholecystokinin-induced excitation in the substantia nigra: evidence for peripheral and central components. *Journal of Neuroscience, 5*(6), 1387-1392.

Hornykiewicz, O. (2002). Dopamine miracle: from brain homogenate to dopamine replacement. *Movement Disorders, 17*(3), 501-508. doi: 10.1002/mds.10115

Howe, M. W., & Dombeck, D. A. (2016). Rapid signalling in distinct dopaminergic axons during locomotion and reward. *Nature, 535*(7613), 505–510. https://doi.org/10.1038/nature18942

Inoue, K. I, Miyachi, S., Nishi, K., Okado, H., Nagai, Y., Minamoto, T., Nambu, A., & Takada, M. (2018). Recruitment of calbindin into nigral dopamine neurons protects against MPTP-induced parkinsonism. *Movement Disorders, 34*(2), 200-209. https://doi-org.ezproxy.library.uvic.ca/10.1002/mds.107

Ito, D., Imai, Y., Ohsawa, K., Nakajima, K., Fukuuchi, Y., & Kohsaka, S. (1998). Microglia-specific localisation of a novel calcium binding protein, Iba1. *Molecular Brain Research, 57*(1), 1-9. https://doi.org/10.1016/S0169-328X(98)00040-0

Jung, E. M., Yoo, Y. M., Park, S. Y., Ahn, C., Jeon, B. H., Hong, E. J., Kim, W. Y., & Jeung, E. B. (2020). Calbindin-D9k is a novel risk gene for neurodegenerative disease. *Cellular Physiology & Biochemistry, 54*(3), 438-456. https://doi.org/10.33594/000000229

Katolikova, N., Gainetdinov, R.R. (2021). Dopamine System. In: Offermanns, S., Rosenthal, W. (eds) *Encyclopedia of Molecular Pharmacology* (p. 554-560) https://doi.org/10.1007/978-3-030-57401-7_51

Kiyama, H., Seto-Ohshima, A., & Emson, P. C. (1990). Calbindin D28K as a marker for the degeneration of the striatonigral pathway in Huntington's disease. *Brain research*, *525*(2), 209–214. https://doi.org/10.1016/0006-8993(90)90866-a

Knowlton, C., Kutterer, S., Roeper, J., & Canavier, C. C. (2018). Calcium dynamics control K-ATP channel-mediated bursting in substantia nigra dopamine neurons: a combined experimental and modeling study. *Journal of neurophysiology*, *119*(1), 84–95. https://doi.org/10.1152/jn.00351.2017

Kojetin, D. J., Venters, R. A., Kordys, D. R., Thompson, R. J., Kumar, R., & Cavanagh, J. (2006). Structure, binding interface and hydrophobic transitions of Ca^{2+}-loaded calbindin-D28k. *Nature Structural and Molecular Biology, 13*, 641-647.

Kravitz, A. V., Freeze, B. S., Parker, P. R. L., Kay, K., Thwin, M. T., Deisseroth, K., & Kreitzer, A. C. (2010). Regulation of parkinsonian motor behaviours by optogenetic control of basal ganglia circuitry. *Nature, 466*, 622-626.

Kravitz, A. V., Tye, L. D., & Kreitzer, A. C. (2012). Distinct roles for direct and indirect pathway striatal neurons in reinforcement. *Nature Neuroscience, 15*(6), 816–818. https://doi.org/10.1038/nn.3100

Lambers, T. T., Mahieu, F., Oancea, E., Hoofd, L., de Lange, F., Mensenkamp, A. R., Voets, T., Nilius, B., Clapham, D. E., Hoenderop, J. G., & Bindels, R. J. (2006). Calbindin-D28K

dynamically controls TRPV5-mediated Ca2+ transport. *The EMBO Journal*, *25*(13), 2978–2988. https://doi.org/10.1038/sj.emboj.7601186

Lawson, L. J., Perry, V. H., Dri, P., & Gordon, S. (1990). Heterogeneity in the distribution and morphology of microglia in the normal adult mouse brain. *Neuroscience, 39*(1), 151-170. https://doi.org/10.1016/0306-4522(90)90229-W

Lee, H. J., Weitz, A. J., Bernal-Casas, D., Duffy, B. A., Choy, M., Kravitz, A. V., Kreitzer, A. C., & Lee, J. H. (2016). Activation of Direct and Indirect Pathway Medium Spiny Neurons Drives Distinct Brain-wide Responses. *Neuron*, *91*(2), 412–424. https://doi.org/10.1016/j.neuron.2016.06.010

Liang, C. L., Sinton, C. M., Sonsalla, P. K., & German, D. C. (1996). Midbrain dopaminergic neurons in the mouse that contain calbindin-D28k exhibit reduced vulnerability to MPTP-induced neurodegeneration. *Neurodegeneration : a journal for neurodegenerative disorders, neuroprotection, and neuroregeneration*, *5*(4), 313–318. https://doi.org/10.1006/neur.1996.0042

Liss, B., Neu, A., & Roeper, J. (1999). The weaver mouse gain-of-function phenotype of dopaminergic midbrain neurons is determined by coactivation of wvGirk2 and K-ATP channels. *The Journal of neuroscience : the official journal of the Society for Neuroscience*, *19*(20), 8839–8848. https://doi.org/10.1523/JNEUROSCI.19-20-08839.1999

Liu, F. C., & Graybiel, A. M. (1992). Heterogeneous development of calbindin-D28K expression in the striatal matrix. *The Journal of comparative neurology, 320*(3), 304–322. https://doi.org/10.1002/cne.903200304

Madisen, L., Mao, T., Koch, H., Zhuo, J. M., Berenyi, A., Fujisawa, S., Hsu, Y. W., Garcia, A. J., 3rd, Gu, X., Zanella, S., Kidney, J., Gu, H., Mao, Y., Hooks, B. M., Boyden, E. S., Buzsáki, G., Ramirez, J. M., Jones, A. R., Svoboda, K., Han, X., … Zeng, H. (2012). A toolbox of Cre-dependent optogenetic transgenic mice for light-induced activation and silencing. *Nature Neuroscience*, *15*(5), 793–802. https://doi.org/10.1038/nn.3078

Martinez Damonte, V., Pomrenze, M. B., Manning, C. E., Casper, C., Wolfden, A. L., Malenka, R. C., & Kauer, J. A. (2023). Somatodendritic Release of Cholecystokinin Potentiates GABAergic Synapses Onto Ventral Tegmental Area Dopamine Cells. *Biological psychiatry*, *93*(2), 197–208. https://doi.org/10.1016/j.biopsych.2022.06.011

McDonald, W. M., Sibley, D. R., Kilpatrick, B. F., & Caron, M. G. (1984). Dopaminergic inhibition of adenylate cyclase correlates with high affinity agonist binding to anterior pituitary D2 dopamine receptors. *Molecular and Cellular Endocrinology, 36*(3), 201-209. https://doi-org.ezproxy.library.uvic.ca/10.1016/0303-7207(84)90037-6

McRitchie, D. A., & Halliday, G. M. (1995). Calbindin-D28k-containing neurons are restricted to the medial substantia nigra in humans. *Neuroscience, 65*(1), 87-91. https://doi.org/10.1016/0306-4522(94)00483-L

Mongia, S., Yamaguchi, T., Liu, B., Zhang, S., Wang, H., & Morales, M. (2019). The ventral tegmental area has calbindin neurons with the capability to co-release glutamate and

dopamine into the nucleus accumbens. *The European Journal of Neuroscience*, *50*(12), 3968–3984. https://doi.org/10.1111/ejn.14493

Nair-Roberts, R. G., Chatelain-Badie, S. D., Benson, E., White-Cooper, H., Bolam, J. P., & Ungless, M. A. (2008). Stereological estimates of dopaminergic, GABAergic and glutamatergic neurons in the ventral tegmental area, substantia nigra and retrorubral field in the rat. *Neuroscience, 152*(4), 1024–1031. https://doi.org/10.1016/j.neuroscience.2008.01.046

Nagano-Saito, A., Leyton, M., Monchi, O., Goldberg, Y. K., He, Y., & Dagher, A. (2008). Dopamine depletion impairs frontostriatal functional connectivity during a set-shifting task. *The Journal of Neuroscience, 28*(14), 3697–3706. https://doi.org/10.1523/JNEUROSCI.3921-07.2008

Nagel, G., Szellas, T., Huhn, W., Kateriya, S., Adeishvili, N., Berthold, P., Ollig, D., Hegemann, P., & Bamberg, E. (2003). Channelrhodopsin-2, a directly light-gated cation-selective membrane channel. *Biophysics and Computational Biology, 100*(24), 12940-13945. https://doi.org/10.1073/pnas.1936192100

Nemoto, C., Hida, T., & Arai, R. (1999). Calretinin and calbindin-D28k in dopaminergic neurons in the rat midbrain: a triple-labeling immunohistochemical study. *Brain Research, 846*(1), 129-136. https://doi.org/10.1016/s0006-8993(99)01950-2

Olson, V. G., & Nestler, E. J. (2007). Topographical organization of GABAergic neurons within the ventral tegmental area of the rat. *Synapse, 61*, 87-95. doi: 10.1002/syn.20345

Onla-or, S., & Winstein, C. J. (2001). Function of the 'direct' and 'indirect' pathways of the basal ganglia motor loop: evidence from reciprocal aiming movements in Parkinson's disease. *Cognitive Brain Research, 10*(3), 329-332. https://doi.org/10.1016/S0926-6410(00)00046-X

Ou, Z., Pan, J., Tang, S., Duan, D., Yu, D., Nong, H., & Wang, Z. (2021). Global trends in the incidence, prevalence, and years lived with disability of Parkinson's disease in 204 countries/territories from 1990 to 2019. *Frontiers in Public Health, 9.* https://doi.org/10.3389/fpubh.2021.776847

Palacios, J. M., Savasta, M., & Mengod, G. (1989). Does cholecystokinin colocalize with dopamine in the human substantia nigra? *Brain Research, 488*(1-2), 369-375. https://doi.org/10.1016/0006-8993(89)90733-6

Palczewski, K., Buczyłko, J., Kaplan, M. W., Polans, A. S., & Crabb, J. W. (1991). Mechanism of rhodopsin kinase activation. *The Journal of biological chemistry*, *266*(20), 12949–12955.

Papenberg, G., Jonasson, L., Karalija, N., Johansson, J., Köhncke, Y., Salami, A., Andersson, M., Axelsson, J., Wåhlin, A., Riklund, K., Lindenberger, U., Lövdén, M., Nyberg, L., & Bäckman, L. (2019). Mapping the landscape of human dopamine D2/3 receptors with [^{11}C]raclopride. *Brain structure & function*, *224*(8), 2871–2882. https://doi.org/10.1007/s00429-019-01938-1

Paxinos, George, and Keith B.J. Franklin. *The mouse brain in stereotaxic coordinates: hard cover edition.* Access Online via Elsevier, 2001.

Poulin, JF., Caronia, G., Hofer, C. *et al.* (2018). Mapping projections of molecularly defined dopamine neuron subtypes using intersectional genetic approaches. *Nature Neuroscience*, *21*, 1260–1271 https://doi.org/10.1038/s41593-018-0203-4

Prabhakar, A., Vujovic, D., Cui, L., Olson, W., & Luo, W. (2019). Leaky expression of channel-rhodopsin-2 (ChR2) in Ai32 mouse lines. *Plos One, 14*(3). https://doi.org/10.1371/journal.pone.0213326

Preibisch, S., Saalfeld, S., & Tomancak, P. (2009). Globally optimal stitching of tiled 3D microscopic image acquisitions. *Bioinformatics*, *25*(11), 1463–1465. doi:10.1093/bioinformatics/btp184

Radu, I., Bamann, C., Nack, M., Nagel, G., Bamberg, E., & Heberle, J. (2009). Conformational changes of channelrhodopsin-2. *Journal of the American Chemical Society, 131*(21), 7313–7319. https://doi.org/10.1021/ja8084274

Rascol, O., Brooks, D. J., Korczyn, A. D., De Deyn, P. P., Clarke, C. E., & Lang, A. E. (2000). A five-year study of the incidence of dyskinesia in patients with early Parkinson's disease who were treated with ropinirole or levodopa. *The New England Journal of Medicine, 342*(20), 1484–1491. https://doi.org/10.1056/NEJM200005183422004

Rcom-H'cheo-Gauthier, A. N., Meedeniya, A. C. B., & Poutney, D. L. 2017. Calcipotriol inhibits alpha-synuclein aggregation in SH-SY5Y neuroblastoma cells by a calbindin-D28k-dependent mechanism. *Journal of Neurochemistry, 41*(2), 263-274. https://doi-org.ezproxy.library.uvic.ca/10.1111/jnc.13971

Reyes, S., Fu, Y., Double, K., Thompson, L., Kirik, D., Paxinos, G., Halliday, G. M. (2012). GIRK2 expression in dopamine neurons of the substantia nigra and ventral tegmental area. *Journal of Comparative Neurology, 520*(12), 2591-2607. https://doi-org.ezproxy.library.uvic.ca/10.1002/cne.23051

Rintoul, G. L., Raymond, L. A., & Baimbridge, K. G. (2001). Calcium buffering and protection from excitotoxic cell death by exogenous calbindin-D28k in HEK 293 cells. *Cell Calcium*, *29*(4), 277–287. https://doi.org/10.1054/ceca.2000.0190

Rogers, J. H., & Résibois, A. (1992). Calretinin and calbindin-D28k in rat brain: patterns of partial co-localization. *Neuroscience, 51*(4), 843-865. https://doi.org/10.1016/0306-4522(92)90525-7

Root, D. H., Wang, H. L., Liu, B., Barker, D. J., Mód, L., Szocsics, P., Silva, A. C., Maglóczky, Z., & Morales, M. (2016). Glutamate neurons are intermixed with midbrain dopamine neurons in nonhuman primates and humans. *Nature Scientific Reports, 6.*

Rubí, B., & Maechler, P. (2010). Minireview: new roles for peripheral dopamine on metabolic control and tumor growth: let's seek the balance. *Endocrinology, 151*(12), 5570-5581. https://doi.org/10.1210/en.2010-0745

Rung, J. P., Carlsson, A., Rydén Markinhuhta, K., & Carlsson, M. L. (2005). (+)-MK-801 induced social withdrawal in rats; a model for negative symptoms of schizophrenia. *Progress in Neuro-Psychopharmacology & Biological Psychiatry, 29*(5), 827–832. https://doi.org/10.1016/j.pnpbp.2005.03.004

Schiemann, J., Schlaudraff, F., Klose, V., Bingmer, M., Seino, S., Magill, P. J., Zaghloul, K. A., Schneider, G., Liss, B., & Roeper, J. (2012). K-ATP channels in dopamine substantia nigra neurons control bursting and novelty-induced exploration. *Nature Neuroscience, 15,* 1272-1280.

Schmidt, H., Schwaller, B., & Eilers, J. (2005). Calbindin D28k targets *myo*-inositol monophosphatase in spines and dendrites of cerebellar Purkinje neurons. *PNAS, 102*(16), 5850-5855. https://doi.org/10.1073/pnas.0407855102

Schmidt H. (2012). Three functional facets of calbindin D-28k. *Frontiers in Molecular Neuroscience, 5*, 25. https://doi.org/10.3389/fnmol.2012.00025

Schultz, W. (1998). Predictive reward signal of dopamine neurons. *Journal of Neurophysiology, 80*(1), 1-27. https://doi.org/10.1152/jn.1998.80.1.1

Schultz, W., Dayan, P., & Montague, P. R. (1997). A neural substrate of prediction and reward. *Science, 275*(5306), 1593-1599. https://doi.org/10.1126/science.275.5306.1593

Smith, J. B., Klug, J. R., Ross, D. L., Howard, C. D., Hollon, N. G., Ko, V. I., Hoffman, H., Callaway, E. M., Gerfen, C. R., & Jin, X. (2016). Genetic-Based Dissection Unveils the Inputs and Outputs of Striatal Patch and Matrix Compartments. *Neuron, 91*(5), 1069–1084. https://doi.org/10.1016/j.neuron.2016.07.046

Stagkourakis, S., Dunevall, J., Taleat, Z., Ewing, A. G., & Broberger, C. (2019). Dopamine Release Dynamics in the Tuberoinfundibular Dopamine System. *The Journal of neuroscience : the official journal of the Society for Neuroscience*, *39*(21), 4009–4022. https://doi.org/10.1523/JNEUROSCI.2339-18.2019

Stefanis L. (2012). α-Synuclein in Parkinson's disease. *Cold Spring Harbor Perspectives in Medicine*, *2*(2), a009399. https://doi.org/10.1101/cshperspect.a009399

Tanaka, S., Ishii, A., Ohtaki, H., Shioda, S., Yoshida, T., & Numazawa, S. (2013). Activation of microglia induces symptoms of Parkinson’s disease in wild-type, but not in IL-1 knockout mice. *Journal of Neuroinflammation, 10*(907).

Tepper, J. M., Martin, L. P., & Anderson, D. R. (1995). GABA-A receptor-mediated inhibition of rat substantia nigra dopaminergic neurons by pars reticulata projection neurons. *Journal of Neuroscience, 15*(4), 3092-3103. https://doi.org/10.1523/jneurosci.15-04-03092.1995

Veenstra, T. D., Johnson, K. L., Tomlinson, A. J., Naylor, S., & Kumar, R. (1997). Determination of calcium-binding sites in rat brain calbindin D28k by electrospray ionization mass spectrometry. *Biochemistry, 36*(12), 3535-3542. https://doi.org/10.1021/bi9628329

Volkow, N. D., Fowler, J. S., Wang, G. J., Hitzemann, R., Logan, J., Schlyer, D. J., Dewey, S. L., & Wolf, A. P. (1993). Decreased dopamine D2 receptor availability is associated with

reduced frontal metabolism in cocaine abusers. *Synapse, 14*(2), 169–177. https://doi.org/10.1002/syn.890140210

Volkow, N. D., Wang, G. J., Kollins, S. H., Wigal, T. L., Newcorn, J. H., Telang, F., Fowler, J. S., Zhu, W., Logan, J., Ma, Y., Pradhan, K., Wong, C., & Swanson, J. M. (2009). Evaluating dopamine reward pathway in ADHD: clinical implications. *JAMA*, *302*(10), 1084–1091. https://doi.org/10.1001/jama.2009.1308

Watabe-Uchida, M., Zhu, L., Ogawa, S. K., Vamanrao, A., & Uchida, N. (2012). Whole-brain mapping of direct inputs to midbrain dopamine neurons. *Neuron, 74*(5), 858-873. https://doi-org.ezproxy.library.uvic.ca/10.1016/j.neuron.2012.03.017

Willing, J., & Wagner, C. K. (2016). Exposure to the synthetic progestin, 17α-hydroxyprogesterone caproate during development impairs cognitive flexibility in adulthood. *Endocrinology, 157*(1), 77-82. https://doi-org.ezproxy.library.uvic.ca/10.1210/en.2015-1775

Willis, A. W., Roberts, E., Beck, J. C., Fiske, B., Ross, W., Savica, R., Van Den Eeden, S. K, Tanner, C. M., & Marras, C. (2022). Incidence of Parkinson's disease in North America. *Nature Partner Journals Parkinson's Disease, 8*(170).

Wüllner, W., Pakzaban, P., Brownell, A. L., Hantraye, P., Burns, L., Shoup, T., Elmaleh, D., Petto, A. J., Spealman, R. D., Brownell, G. L., & Isacson, O. (1994) Dopamine terminal loss and onset of motor symptoms in MPTP-treated monkeys: a positron emiition tomography study with 11C-CFT. *Experimental Neurology,* 126(2). https://doi.org/10.1006/exnr.1994.1069

Yamada, T., McGeer, P. L., Baimbridge, K. G., & McGeer, E. G. (1990). Relative sparing in Parkinson's disease of substantia nigra dopamine neurons containing calbindin-D28k. *Brain Research, 526*(2), 303-307. https://doi.org/10.1016/0006-8993(90)91236-A

Yamaguchi, T., Sheen, W., & Morales, M. (2007). Glutamatergic neurons are present in the rat ventral tegmental area. *The European journal of neuroscience*, *25*(1), 106–118. https://doi.org/10.1111/j.1460-9568.2006.05263.x

Yamaguchi, T., Wang, H. L., & Morales, M. (2013). Glutamate neurons in the substantia nigra compacta and retrorubral field. *The European journal of neuroscience*, *38*(11), 3602–3610. https://doi.org/10.1111/ejn.12359

Yu, X., Li, W., Ma, Y., Tossell, K., Harris, J. J., Harding, E. C., Ba, W., Miracca, G., Wang, D., Li, L., Guo, J., Chen, M., Li, Y., Yustos, R., Vyssotski, A. L., Burdakov, D., Yang, Q., Dong, H., Franks, N. P., & Wisden, W. (2019). GABA and glutamate neurons in the VTA regulate sleep and wakefulness. *Nature neuroscience*, *22*(1), 106–119. https://doi.org/10.1038/s41593-018-0288-9

Zell, V., Steinkellner, T., Hollon, N. G., Warlow, S. M., Souter, E., Faget, L., Hunker, A. C., Jin, X., Zweifel, L. S., & Hnasko, T. S. (2020). VTA Glutamate neuron activity drives positive reinforcement absent dopamine co-release. *Neuron*, *107*(5), 864–873.e4. https://doi.org/10.1016/j.neuron.2020.06.011

Zenchak, J. R., Palmateer, B., Dorka, N., Brown, T. M., Wagner, L. M., Medendorp, W. E., Petersen, E. D., Prakash, M., & Hochgeschwender, U. (2018). Bioluminescence-driven optogenetic activation of transplanted neural precursor cells improves motor deficits in a Parkinson's disease mouse model. *Journal of Neuroscience Research, 98*, 458-468. doi: 10.1002/jnr.24237

Zhang, Z., Li, H., Su, Y., Ma, J., Yuan, Y., Yu, Z., Shi, M., Shao, S., Zhang, Z., Hölscher, C. (2022). Neuroprotective effects of a cholecystokinin analogue in the 1-methyl-4-phenyl-1,2,3,6-tetrahydropyridine Parkinson's disease mouse model. *Neuroscience, 16.* https://doi.org/10.3389/fnins.2022.814430

Zhou, Q. Y., Grandy, D. K., Thambi, L., Kushner, J. A., Van Tol, H. H., Cone, R., Pribnow, D., Salon, J., Bunzow, J. R., & Civelli, O. (1990). Cloning and expression of human and rat D1 dopamine receptors. *Nature*, *347*(6288), 76–80. https://doi.org/10.1038/347076a0

Zinchenko, V. P., Kosenkov, A. M., Gaidin, S. G., Sergeev, A. I., Dolgacheva, L. P., & Tuleukhanov, S. T. (2021). Properties of GABAergic Neurons Containing Calcium-Permeable Kainate and AMPA-Receptors. *Life (Basel, Switzerland)*, *11*(12), 1309. https://doi.org/10.3390/life11121309

Figures 1, 2, and 3 were created using **BioRender.com.**

7.0 Appendix

Table 1. Calculation of colocalization percentages. Data for each brain region consisted of counts from a total of 27 images of the MSNc, LSNc, and VTA of both hemispheres of from four mice (n = 8).

	Brain Region	Number of ROIs	% Colocalized (mean ± SE)	Statistical tests and values
% TH+CALB+/TH+	LSNc	11	6.62 ± 2.48	Kruskal-Wallis Rank Sum Test df = 2, chi-squared = 16.595, $p = 2.491\times10^{-4}$ Dunn's Test LSNc – MSNc, $p = 0.191$ LSNc – VTA, $p = 1.940\times10^{-4}$ MSNc – VTA, $p = 0.014$
	MSNc	8	18.56 ± 5.49	
	VTA	8	59.87 ± 3.60	
% TH+CALB+/CALB+	LSNc	11	26.47 ± 6.80	Single-factor ANOVA df = 2, F = 1.95, $p = 0.17$ Tukey-Kramer Test LSNc – MSNc, $p = 0.59$ LSNc – VTA, $p = 0.14$ MSNc – VTA, $p = 0.60$
	MSNc	8	34.47 ± 4.59	
	VTA	8	42.31 ± 5.41	
% TH+CHR2/TH+	LSNc	11	98.33 ± 0.64	No comparison tests performed.
	MSNc	8	96.89 ± 0.63	
	VTA	8	95.73 ± 0.77	